Effect of Mg Doping on Physical Properties of NiCr$_2$O$_4$ Nanoparticles

by:

Irfan Ahmed
(357-FBAS/MSPHY/F15)

Supervisor:

Dr. Kashif Nadeem

Assistant Professor

Department of Physics, FBAS,

IIUI, Islamabad

Department of Physics

Faculty of Basic and Applied Sciences

International Islamic University, Islamabad

(2017)

MS
620.5
IRE

Nano technology

Nanoparticles

X - Ray - diffraction

Nanotechnology

Nanoparticles

X-Ray-diffraction

Magnetic properties

Effect of Mg Doping on Physical Properties of NiCr₂O₄ Nanoparticles

by:

Irfan Ahmed
(357-FBAS/MSPHY/F15)

This Thesis submitted to Department of Physics International Islamic University Islamabad, for the award of degree of
MS Physics.

CHAIRMAN
DEPT OF PHYSICS
International Islamic University
Islamabad

Chairman, Department of Physics
International Islamic University, Islamabad

M. Ahmad

Dean Faculty of Basic and Applied Science
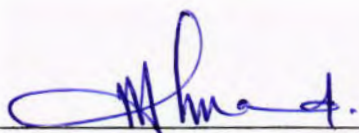**International Islamic University, Islamabad**

Department of Physics
Faculty of Basic and Applied Sciences
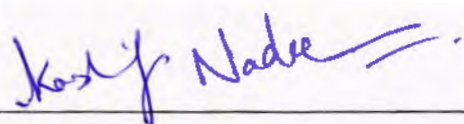**International Islamic University, Islamabad**

Final Approval

It is certified that the work printed in this thesis entitled "**Effect of Mg Doping on Physical Properties of NiCr$_2$O$_4$ Nanoparticles**" by **Irfan Ahmed**, registration No.357-FBAS/ MSPHY/ F15 is of sufficient standard in scope and quality for award of degree of MS Physics from Department of Physics, International Islamic University, Islamabad, Pakistan.
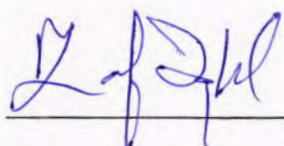
Viva Voce Committee

Chairman (Physics) _____

Supervisor _____

External Examiner _____

Internal Examine _____

بسم الله الرحمن الرحيم

DEDICATED

to

My beloved

Parents

and

My

Respected teachers

Declaration

I **Irfan Ahmed** (Registration # 357-FBAS/MSPHY/F15), student of MS in Physics (Session 2015-2017), here declare that the matter printed in the thesis titled **"Effect of Mg Doping on Physical Properties of NiCr$_2$O$_4$ Nanoparticles"** is my own work and has not been published or submitted as research work or thesis in any form in any other university or institute in Pakistan or aboard.
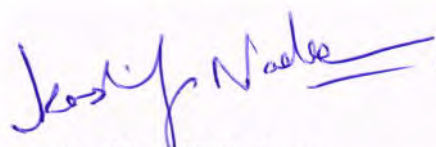
Irfan Ahmed

(357-FBAS/MSPHY/F15)

Dated: _____

Forwarding Sheet by Research Supervisor

The thesis entitled **"Effect of Mg Doping on Physical Properties of NiCr$_2$O$_4$ Nanoparticles"** submitted by **Irfan Ahmed** in partial fulfillment of M.S. degree in Physics has been completed under my guidance and supervision. I am satisfied with the quality of student's research work and allow him to submit this thesis for further process to graduate with Master of Science degree from Department of Physics, as per IIU rules and regulations.

Dated: _____

Dr. Kashif Nadeem
Assistant Professor
Department of Physics,
International Islamic University,
Islamabad.

Acknowledgment

First, I owe my deepest gratitude to **Allah** Almighty for all of his countless blessings. I offer my humblest words of thanks to his most noble messenger **Hazrat Muhammad (P.B.U.H)**, who is forever, a torch of guidance and knowledge for all humanity. By virtue of his blessings today I am able to carry out our research work and present it.

I would like to acknowledge the worth mentioning supervision of **Dr. Kashif Nadeem** who guided me and supported me during my whole research work. Without his guidance, it was not possible for me to complete my MS. Almighty **Allah** blessed them in every part of life. Moreover, I would like to express my sincere thanks to all the faculty members department of physics IIUI Islamabad specially to Prof. Dr. Mushtaq Ahmed (Chairman)

I particularly want to acknowledgment effectors and prayed of my parents. I offer my cordial thanks to my brother Naseer Ahmed, M. Nazarat, and sisters for their love, sincerity, prayers, encouragement and best Co-operation. How can I forget the Joyful company, great help and best co-operation of my loving and sweet friends, Sajid Elahi, Ghazanfar Mehboob, Zahid Shafiq, Danyal Ahmed, Usman Amin, Wahid Raiz, Ziafat Ali Shah, Nasir Iqbal Awais Ahmed, whom I share unforgettable moments of pleasure, anxiety and accomplishment, It will be unfair not be pay thanks to my classmates and research colleagues Zaeem-Ul-Hassan, Aqib Javed, Ishaq khan, Noman Saeed, & all other fellows.I am also thankful to Phd scalor Fasial Zeb, M.Kamran, Hur Abbas ,Khalid Khan & other lab fellows for their great co-operation, sincere and affectionate guidance May Allah almighty shower blessings on those associates me in any way during completion of this project. (Ameen)

Irfan Ahmed.

Contents

.

List of figures

List of tables

Abstract

We have synthesized Mg doped nickel chromite ($Ni_{1-x}Mg_xCr_2O_4$) nanoparticles with doping of different concentration of Mg (x=0, 0.2, 0.4, 0.6, 0.8 and 1) and studied the effect of doping on the structural, optical, magnetic and dielectric properties. The average crystallite size was obtained by using Debye-Scherrer's formula and was in the range 26-42 nm for different concentration of Mg. X-ray diffraction (XRD) confirmed the cubic structure of $NiCr_2O_4$ and showed no impurity phases, which signifies the formation of single-phase nanoparticles. The average particle size showed an increasing trend with Mg concentration. Transmission electron microscopy (TEM) results confirmed that particles are less agglomerated and non-spherical in shape. Fourier transform infrared spectroscopy (FTIR) analysis showed two frequency bands in the range of 495 to 530 cm^{-1} (Ni-O & Mg-O) and 617 to 651 cm^{-1} (Cr-O) which were the characteristic peaks of $Ni_{1-x}Mg_xCr_2O_4$. M-H loop of $NiCr_2O_4$ showed that the value of saturation magnetization (M_s = 4.65 emu/g) was less than that of bulk value due to finite size effects and the value of coercivity was19407 Oe which proved that they are act as tiny hard magnets. ZFC curve exhibits negative magnetization form 5 K to 87 K, which is due to compensating spins at grain boundaries. Dielectric parameters showed a non-monotonous behavior with Mg concentration and this behavior of dielectric parameters has been explained by using Koop's theory and Wagner's model. Dielectric properties were improved for x = 0.2 and also average particle size is larger for this concentration.

Chapter 1

Introduction

1.1   History of material

Stone Age, followed by Bronze Age and then the Iron Age, so what should we call the next?? Some people named the present period as atomic or space age. However, in our daily lives, nuclear reactor and space exploration haven't set too much impact. In its place, the electrical and electronic devices (telephone, television, radio, electric light, computer, refrigerator, electrometer, CD player, etc.) have too much saturated our daily life. Nowadays, it is unthinkable to spent life in this advance world without presence of electronic devices. Hence, the present era could be named as "Electricity Age". Since, earlier eras were named on that material which played a vital role in the lives of humans, so it may be best to stamp the name of "Electronic Age" to the present period of time.

Therefore, researchers are always in contact to more effective electronic materials, such as insulators, semiconductors, conductors, optically transparent materials, opaque substances and ferromagnetic materials. All the effective properties of these electronic materials are described and ruled by electrons. In fact, if we want broad sense of understanding about the term electronic materials and their relevant properties, then we will have to comprise all those phenomena in which electrons have an active role. Definitely, this is the case for other phenomena such as electrical, magnetic and even several thermal phenomena.

Hence, electronic materials have a significant role in information related technologies and advancement of all devices due to their versatile structural and major physical properties including optical, thermal and magnetic properties. Electronic materials are classified on the basis of their electrical properties i.e. insulators, conductors, semiconductors and superconductors as shown in Figure 1.1. The main objectives of this chapter are to discuss electronic materials in the presence of applied field and specially focused on their magnetic and dielectric features because of their increasing importance in

various research fields such as material science, absorber developments, microwave circuit designs, etc.
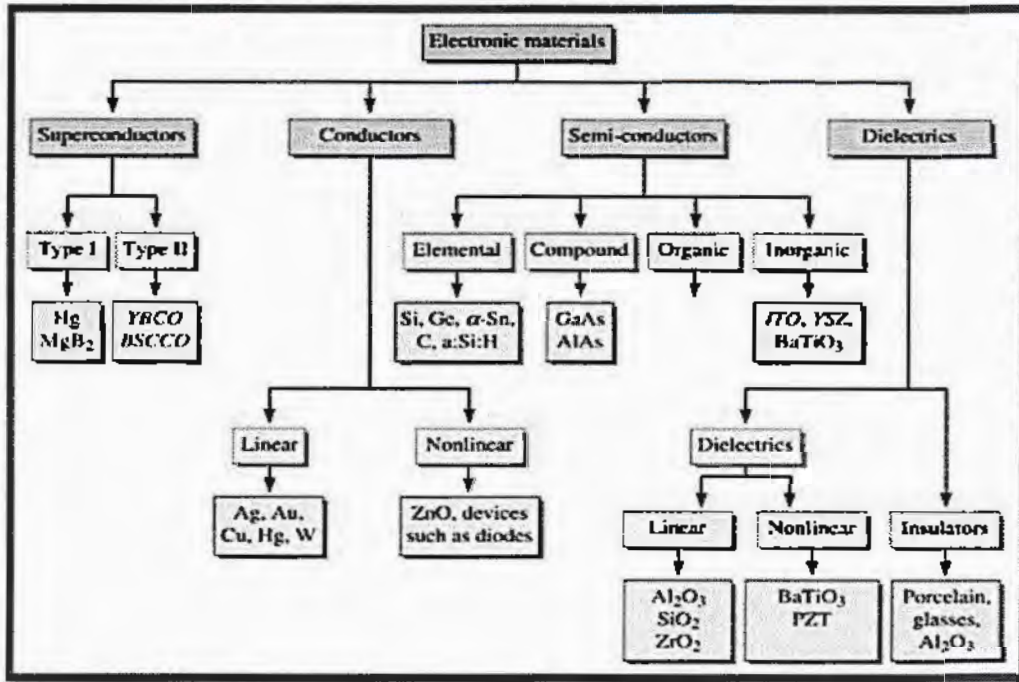
Fig. 1.1: Classification of technologically useful materials [1]

1.2   Nanotechnology

Nanotechnology is a study of small size materials or small size structure having dimension ranging from sub nanometer (nm) to few hundred nanometer (nm) or the technology used for fabrication, design and application of nanomaterials and nanostructures is also known as nanotechnology [2]. If we aligned five silicon or ten hydrogen atoms in a line they are equal to one nanometer. At microlevel material shows almost same properties as bulk but at nanometer scale may shows properties to typically different as compared to bulk [3]. The crystals stables at high temperature and also stable at very low temperature when we go to nanometer scale so ferromagnetism and ferroelectricity of material may also lose [4].

The materials having at least one dimension in nanometer size are known as nano structured materials i.e. quantum dots, nanoparticles, nanowires, nanorod etc. Nano structured materials classified in four categories [5]; zero dimensional (quantum dots and

clusters), one dimensional (nanotubes and nanowires), two dimensional (thin films), and three dimensional (box-shaped graphene).

1.3   Magnetism

The phenomena in which a material shows the property of attraction or repulsion under the effect of magnetic field is called magnetism [6]. The phenomena of magnetism is observed about 2500 years ago and many devises are work on this phenomena like transformers, electric motors,[7] computer, data storage etc. The ratio of volume to dipole moment is known as magnetization (M).

1.3.1 Origin of magnetism

The spin and orbital motion of an electron in an atom is responsible for magnetism as shown in Fig. 1.2. In the external applied field when the orbital and spin motion of electron in atom has same direction so they support each other as a result strong magnetization is produced. Nickel, cobalt are good examples of magnetic material.
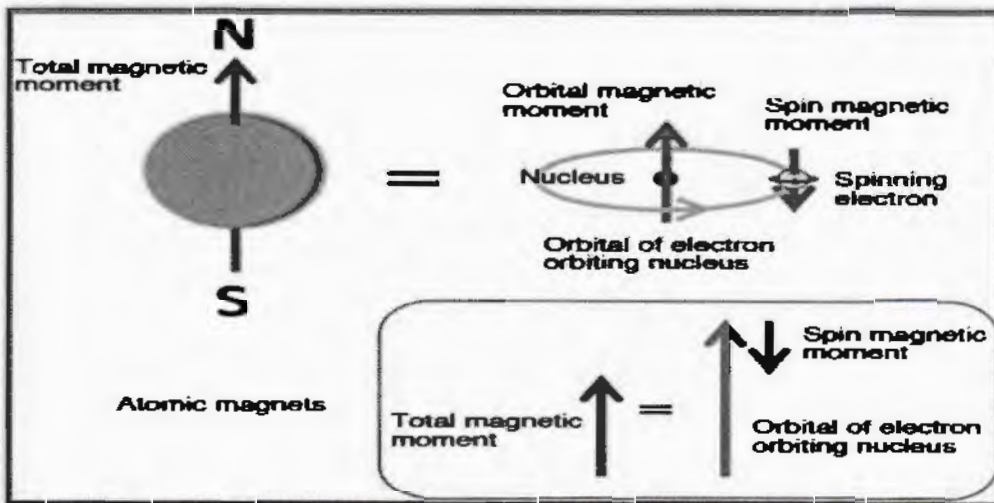
Fig. 1.2: Orbital and spin motion of electron in an atom [8].

1.3.2 Diamagnetism

Almost all materials show a diamagnetic response simply we can define these materials as "Materials in which orbital and spin motion of an electron are oriented in such a way that they cancel their effects and as a result these materials have zero net magnetization are known as diamagnetic materials". The noble gases argon, helium, neon is good example of the diamagnetic material because there outer most shell is completely filled [9]. Also, some diatomic gases show the diamagnetic behavior because they have paired electron in molecular orbitals which vanishes the magnetic moments. The diamagnetic material does not have large number of applications as compared to other type of magnetic materials because they have no permanent magnetic moments. The susceptibility of diamagnetic material is negative. Recently another application of diamagnetic material is placement of liquid crystals by magnetic-field-induced [10]. Diamagnetism is easy to guess and superconductor are also diamagnets because of the Meissner effect [11] there are some metal's which shows diamagnetic behavior. Diamagnetic material response in presence and absence of applied field is shown in Fig. 1.3.
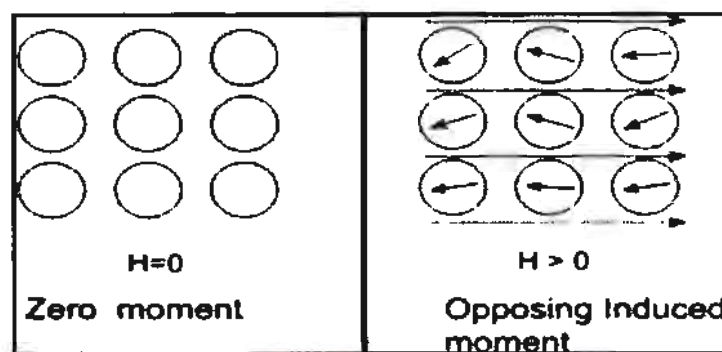
Fig. 1.3: Diamagnetic material response in presence and absence of applied field [12].

1.3.3 Paramagnetism

Those material's in which orbital and spin motion of electrons support each other and as a result some magnetization is observed are known as paramagnetic materials and the phenomenon is known as paramagnetism. The magnetic moments in paramagnetic materials are very feebly coupled and by thermal agitation these are aligned in random

direction. Some magnetic moments are start alignments when an external field is applied but only miner deflection in direction of field is observed for all field strengths. The transition elements of the salts, rare earth salts, aluminum, oxygen etc. are the examples of paramagnetic materials. If the thermal energy is high enough all the ferromagnetic become paramagnetic material above the curie temperature. The value of susceptibility is somewhat greater the zero its value lies in the range of around 10^{-3} and 10^{-5}. In some cases, there is an inverse relationship between susceptibility and temperature. The Langevin localized-moment model explain the dependence of χ on the temperature[13].In paramagnetic materials atoms contains permanent dipole moments. When the field is zero the magnetic moments are randomly distributed and small magnetization is produced   by applied field H as shown in Fig.1.4.
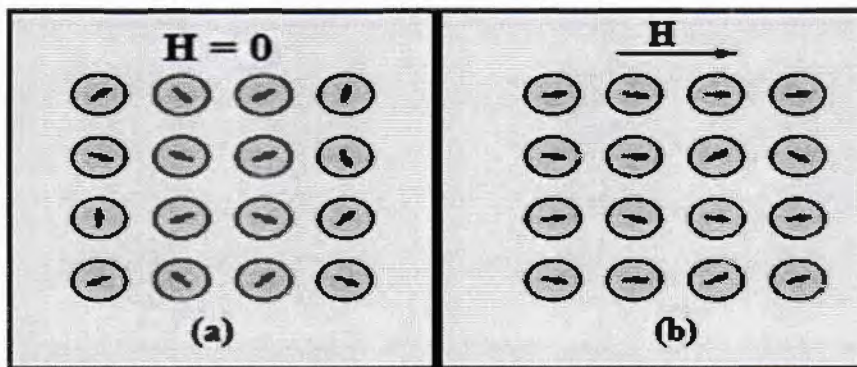
Fig. 1.4: Response of paramagnetic material in an applied magnetic field H [14]

1.3.4   Ferromagnetism

Ferromagnetic materials are those materials in which magnetic moments are due to strong internal interactions, which are line up and produced a spontaneous magnetization. In this type of material, the moments align similar or in same fashion, as a result net magnetization is produced. The value of susceptibility can also be very large and is every so often hysteretic because in this type of material magnetization produced via motion of domains walls. The ferromagnetic material becomes the paramagnetic material above a temperature known as Curie temperatures, T_c. The exchange interactions are present in ferromagnetic material for the reason that the overlapping of ionic and atomic

5

molecules [15]. Below the temperature known as curie temperature spontaneous magnetization arises and the material changed to paramagnetic above the curie temperature [14]. The frequently used ferromagnetic are Nickle (Ni), iron (Fe) etc. Response of ferromagnetic material with and without field is shown in Fig. 1.5.
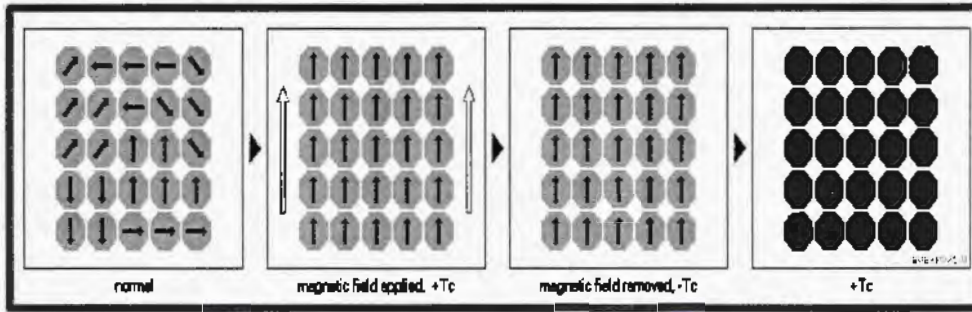
Fig. 1.5: Response of ferromagnetic material with and without field [16].

In ferromagnetic materials exchange interaction are due to huge number of small regions present in the material known as domains. The wall present between the two adjacent domains is known as domain wall or Bloch wall and each domain comprise of 10^{15} to 10^{16} atoms. In each domain, the direction of moments is same which enhance the magnetization.

1.3.5 Antiferromagnetism

In antiferromagnetic material, net magnetization is zero because magnetic moments are equal and reverse in direction as a result cancel the effect of one and other. In antiferromagnetism the interaction of magnetic moments has a tendency to align moments antiparallel. The antiferromagnets consist of two alike and interpenetrating sub lattices of ion or magnetic ions. At critical temperature (Neel temperature T_N) one set of these ions spontaneously magnetized in one direction and other set is also magnetized spontaneously in opposite direction by the same amount. So antiferromagnets have no net magnetization and shows a similar response as like paramagnetic material at a fixed temperature in an applied external field. In antiferromagnetic susceptibility has very small but positive value and magnetization shows a liner behavior in applied external field. These materials have value susceptibility same as the paramagnet materials above the Neel temperature and below it decreases with temperature. Transition metals oxides are good example of

antiferromagnetism as well as other compound such as selenides and sulphides [17].
Antiferromagnetic spin order is shown in Fig. 1.6.
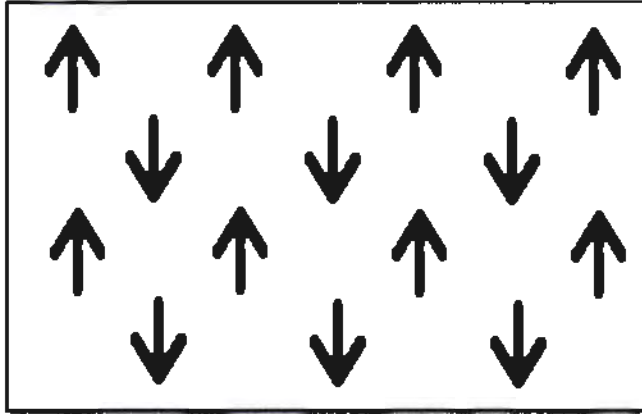
Fig. 1.6: Antiferromagnetic spin order [18].

1.3.6 Ferrimagnetism

The behavior of ferrimagnets is microscopically almost same as of ferromagnets because they show a spontaneous magnetization below a temperature known as T_c (critical temperature) even without any field. But these two types of materials have a distinctly different magnetization curve because ferrimagnet materials are also linked to antiferromagnets materials and antiparallel alignment of magnetic ions due to exchange coupling between magnetic ions. The net magnetization is produced because these two lattice has different magnitude of magnetic moments. In the macroscopic scale ferrimagnets materials are same like ferromagnetic materials having large susceptibility. Mixed oxides of iron such as Fe_2O_3 (maghemite) and Fe_3O_4 (lodestone or magnetite) are good example of the ferrimagnetic materials [19]. Ferrimagnetic spin order is shown in Fig. 1.7.
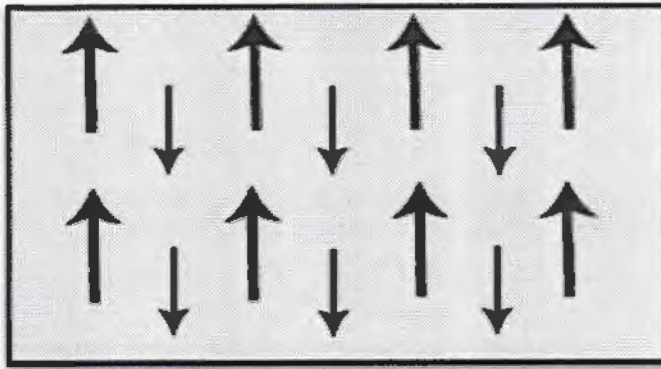
Fig. 1.7: Ferrimagnetic spin order [20].

1.4 Ferrites

These are ferrimagnetic oxides so are electrically insulating. Ferrite is a ceramic material formed by reacting metal-oxide in to a magnetic material. Ferrite is hard and brittle. According to their structure ferrites are divided in to spinel, garnets and hexagonal ferrites. These are widely used in high-frequency applications. Ferrites are classified into two types on the basis of their properties like coercivity, remanence or magnetization.

- Soft ferrites
- Hard ferrites

1.4.1 Soft ferrites

Soft ferrites are ceramic materials, cubic in structure, black or dark gray in color and very hard and brittle. The electrical and magnetic properties are the result of interactions between ions of metals inhibiting particular positions relative to the oxygen ions in its spinel crystalline structure. Soft ferrites are more advantageous over other magnetic materials due to low coercivity, high permeability, stability over a wide temperature range, inherent high resistivity which results in low eddy current losses over wide frequency ranges[21]. Due to these factors, soft ferrites should have narrowed hysteresis loop as shown in Fig. 1.8. On the basis of chemical composition soft ferrites are divided into two

8

main categories; (Mn-Zn) ferrites and (NiZn) ferrites. In both cases, by changing the chemical composition of the elements, variety of materials can be prepared [22].
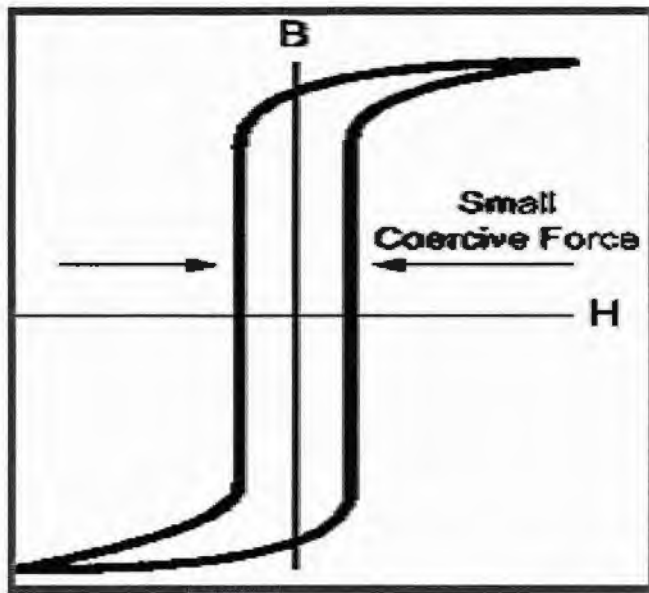
Fig. 1.8: Hysteresis loop of soft ferrites [23].

1.4.1.1 Applications of soft ferrites

Soft ferrite magnets are used at large scale in variety of applications as given below:

- Recording heads
- Magnetic deflection structures
- Transducers
- Data storage and media
- Transformers and chokes
- Telephones, radios, televisions, etc.

1.4.2 Hard ferrites

Hard ferrites are used as a permanent magnet. They have large values of saturation magnetization, remanence and coercivity which imply that the hysteresis loop covers large area as depicted in Fig. 1.9. Hard ferrites are mostly hexagonal compounds with the general formula, $MFe_{12}O_{19}$, where M = Ba, Sr, or Pb. Due to low cost, high chemical stability and

9

availability as raw materials they play an important role in the magnetic industry [24]. These magnets have large magnetic anisotropy and magnetic domain rotations are not easy in such materials. Barium, Strontium and Cobalt are the examples of hard ferrites.
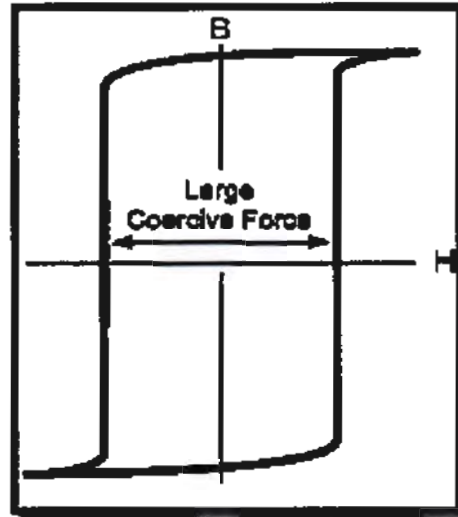
Fig. 1.9: Hysteresis loop of hard ferrites

1.4.2.1 Application of hard ferrites

Hard ferrites are very important in daily life applications, especially in cases where the temperature of device is raised than that of room temperature. Due to raise in temperature of these ferrite magnets, their chemical stability and coercivity increases instead of decreasing [25].

- Door-catches and decorative magnets
- Automobiles
- DC motors
- Windscreen wiper motors
- Household appliances
- Magnetic strips, etc.
- Loudspeakers.

There are generally three main types of ferrites i.e. spinel, Hexagonal and garnet. Here we discuss only spinel ferrites.

1.5   Spinel ferrites

The general formula of spinel's structures is AB_2O_4, where A and B are divalent and trivalent cations, respectively and has a space group Fd3m. These types of structure attracted much attraction due to there tremendous application in the different field of study. There are three different cation arraignments between the sites. A part of spinel unit cell is shown in Fig. 1.10.
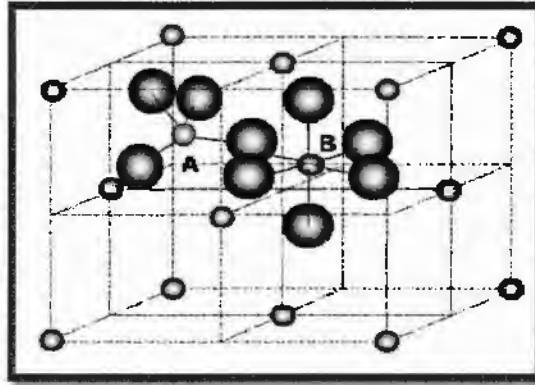
Fig. 1.10: Spinel unit cell showing A-ions on tetrahedral sites and B-ions on octahedral sites [26].

1.5.1 Tetrahedral sites

In a tetrahedral (A) site, metallic ion or interstitial atom is surrounded by four oxygen atoms as presented in Fig. 1.11. In an FCC spinel structure, there are 64 tetrahedral sites and 1/8 of them are occupied by divalent cations (Fe^{2+}). In AB_2O_4, 'A' and 'B' can be divalent, trivalent, or quadrivalent cations, including magnesium, zinc, iron, manganese, aluminum, chromium, titanium and silicon.

11
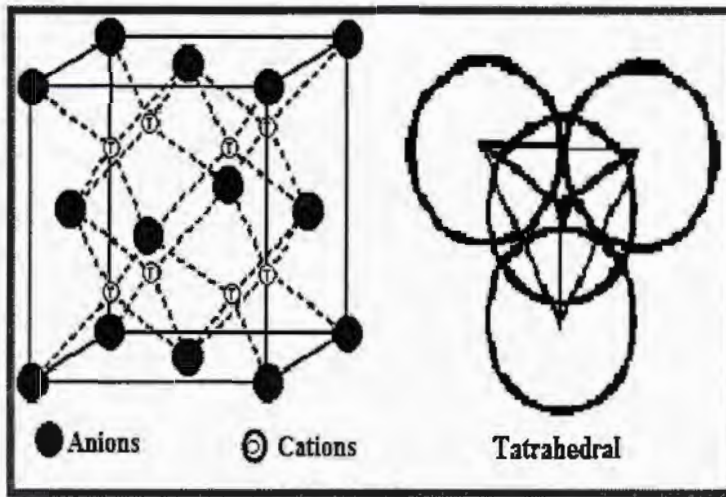
Fig. 1.11: The arrangement of anions. The cell 'owns' 8 tetrahedral sites [26].

1.6   Type of spinel ferrites

There are basically three types of spinel ferrites.

1.6.1   Normal spinel

In normal cubic spinel structure Fd3m, B^{3+} ions reside octahedral sites and A^{2+} ions tetrahedral sites. This type of distribution is observed in spinel zinc chromites $Zn^{2+}Cr^{2+}Cr^{3+}O_4{}^{2-}$. Normal spinel cationic distribution is shown in Fig. 1.12.
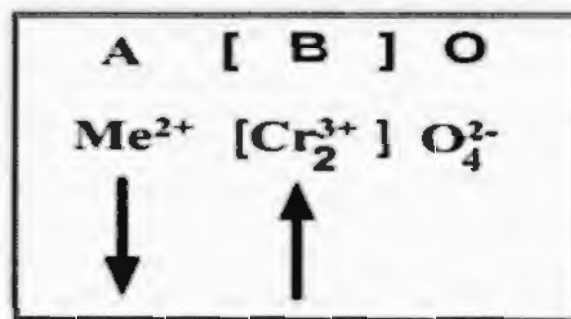
Fig. 1.12: Normal spinel cationic distribution.

1.6.2 Inverse spinel

In inverse crommite , all the A^{2+} ions occupy the octahedral and half of the B^{3+} ions move to the tetrahedral position. The divalent metallic cations play an important role in the magnetic moment and this type of spinal magnetic moments are mutually compensated $Cr^{3+}[Me^{2+}Cr^{3+}]\,O_4^{2-}$. Inverse spinel cationic distribution is shown in Fig. 1.13.
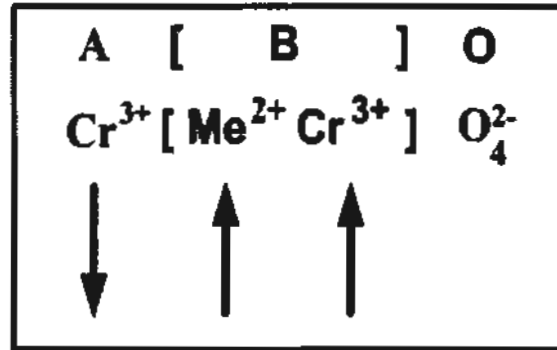
Fig. 1.13: Inverse spinel cationic distribution.

1.6.3 Mixed spinel

In mixed spinel, the cations Ni^{2+} and Cr^{3+} occupies both A and B sites; this chromites have structural formula of $Me_{1-\delta}^{2+}Cr_\delta^{3+}[Me_\delta^{2+}Cr_{2-\delta}^{3+}]\,O_4^{-2}$, where the degree of inversion is given by δ. Fig. 1.14 shows the arrangement in mixed spinel chromites.
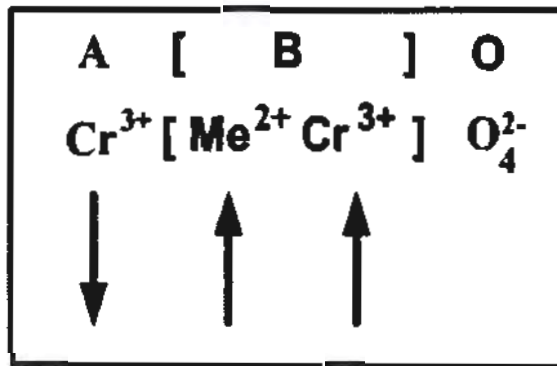
Fig. 1.14: Mixed spinel cationic arrangement.

1.7   Spinel group

The spinel group is basically the class of minerals having general formula of AB_2O_4, which belongs to isomeric cubic crystal structure, where 'A' and 'B' are the metal cations

which usually occupy the tetrahedral and octahedral lattice sites [27]. Some important spinel compounds are listed below in Table 1.1.

Table 1.1: Some important spinel compounds.

Aluminum Spinels	Iron Spinels	Other Spinels
MgAl$_2$O$_4$: Spinels	FeMn$_2$O$_4$: Frankilite	FeCr$_2$O$_4$: Chromite
BeAl$_2$O$_4$: Chrysoberyl	MnFe$_2$O$_4$: Jacobsite	ZnCr$_2$O$_4$: Zinc chromite
ZnAl$_2$O$_4$: Gahnite	Fe$_2$O$_3$: Magnitie	Fev$_2$O$_4$: Coulsinite
MnAl$_2$O$_4$: Galaxite	ZnFe$_2$O$_4$: Zinc ferrite	(Mg,Fe)$_2$SiO$_4$:Ringwoodnite
(Mg,Fe)Al$_2$O$_4$: Trerorite	NiFe$_2$O$_4$: Pleastate	ZnAl$_2$O$_4$: Zinc Aluminate

1.8   Material of choice

Ferrites have been among attractive materials because of their numerous technological applications, for example in electrical devices, sensors, transformers, microwave devices and information storage media[28]. In particular, ferrites with general formula AFe$_2$O$_4$, where A is a divalent cation (Co^{2+}, Mg^{2+}, Ni^{2+}, Mn^{2+}, etc.), having face centered cubic (FCC) structure, is an important class of compounds due to their interesting electrical and magnetic properties, like high electrical resistivity and high magnetic permeability, respectively [29]. Low dielectric and magnetic losses make these materials feasible to be used in electrical devices such as transformers [30].In order to meet the demand for the progress of the miniaturization in electronic devices with more capacity and higher speed, it requires new techniques and new materials. In this research work, nickel chromite (NiCr$_2$O$_4$) has been selected due to its unique and application oriented novel properties. The effects of magnesium (Mg^{2+}) ions incorporated at Ni-site on the structural parameters and thermally assisted electro-active regions in Ni$_{1-x}$Mg$_x$Cr$_2$O$_4$ (x = 0.0, 0.2, 0.4, 0.6, 0.8 & 1.0) compositions has been studied.

1.8.1 Nickel chromite

As nickel chromite is spinel structure. The general formula of spinels structures is AB_2O_4 where A and B are divalent and trivalent cations respectively and has a space group Fd3m [31]. This type of structure attracted much attraction due to there tremendous application in the different field of study because of their potential and magnetic application. The structure between normal and totally inverted structure may form the spinel type compound so we define an inversion parameter by which we can determine a part of B^{3+} cations on tetrahedral sites [32]. The properties of spinel structure are effected by the arrangements and the nature of ions in spinel structure.

1.9   Electric dipole (μ_e) and polarization (P)

An electric dipole comprises of two equal and opposite point charges that are separated by small distance d as shown in Fig. 1.15. The resulting dipole moment is the product of magnitude of either of the charges and the distance between them.

$$\mu_e = q.d \qquad \dots\dots\dots\dots\dots\dots\dots\dots\dots\dots\dots (1.1)$$

Dipole moment is a vector quantity which points from positive to negative charge. It has unit of C-m.
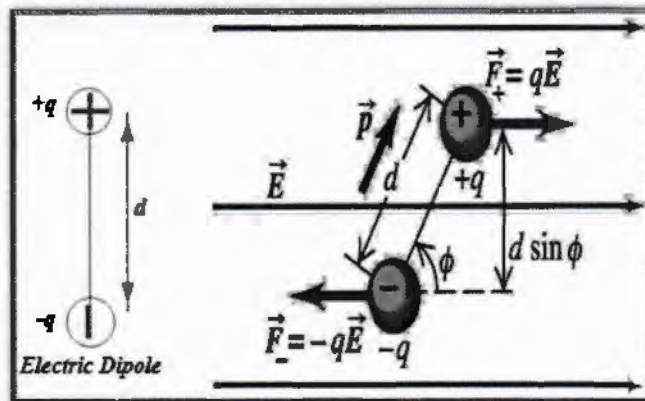
Fig. 1.15: Schematic diagram of electric dipole and dipole moment [33].

Polarization is basically the process of producing electric dipoles by applying an electric field. Mathematically, polarization is defined as the net dipole moment per unit volume.

$$P = \frac{\sum \mu_e}{V} \qquad \dots\dots\dots\dots\dots\dots\dots\dots\dots\dots\dots (1.2)$$

15

Its unit is $C\ m^{-2}$, means charge per unit area. In the most simplistic way, when all the dipoles are aligned in a single direction, then p can be written as N-m (N is the number of dipoles per unit volume). It should be noted that $P = 0$ doesn't mean that there are no dipole moments. It means that the vector sum of all the dipole moments is zero, which is the case where dipoles are randomly distributed [34].
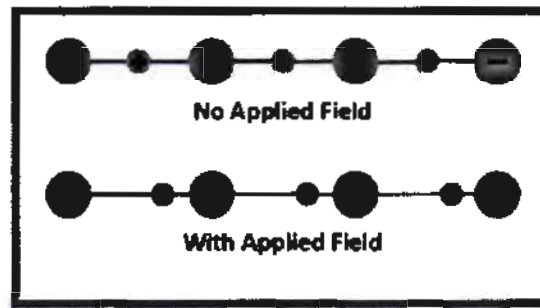
Fig. 1.16: Electric polarization [35]

1.9.1 Mechanisms of electric polarization

In the absence of an external field, ultimately all the materials comprise of charged particles (negative and positive) at atomic level, which cancel out each other's effect macroscopically and give rise to charge neutrality. With the application of an external electric field, the charge neutrality is disturbed by following polarization mechanisms as described below in detail [36].

1.9.2 Electronic and atomic polarization

When an atom (neutral atom) is subjected to an external electric field, its nucleus displaces in the field direction with respect to electron cloud surrounding it as denoted in Fig. 1.17. Such phenomenon is known as electronic polarization. However, atomic polarization take place when an applied field stretches the adjacent negative and positive ions. These polarizations dominate at microwave frequency range for several dry solids. By definition, these polarizations are present in almost all materials and the presence of any other polarization mechanism would be counted an addition [37].
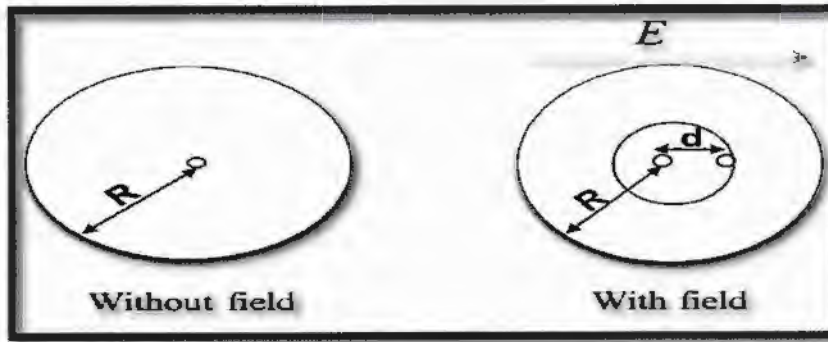
Fig. 1.17: Schematic of electronic polarization [38].

1.9.3 Ionic polarization

This type of polarization is observed in solids when molecules of different atoms asymmetrically share their electrons and the electronic cloud shift towards more electronegative atom as shown in Fig. 1.18. The applied field displaces these charges from their equilibrium positions leading to a net dipole moment i.e. ionic polarization.
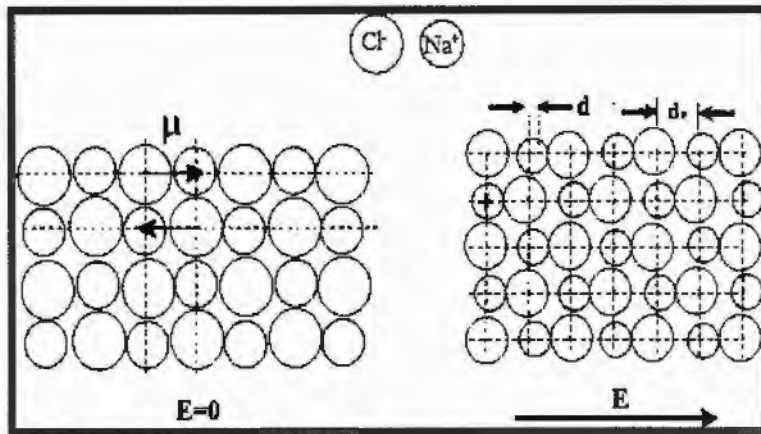
Fig. 1.18: Schematic of ionic polarization in NaCl [39].

In an ionic solid, it is clear that the net dipole moment (from each pair of Cl^- and Na^+ ions) is zero in the absence of an external field due to crystal symmetry. It should also be remembered that dipole rotation is not permissible in ionic solids. However, when an external electric field E is applied, the ions experience a force that move them from their initial equilibrium position, as depicted in the Figure, giving rise to net dipole moment.

We see that the distance between ions increased in one direction by d and decreased by d in the reverse direction. Let F_1 be the force experienced by charges in increasing distance direction and is given by:

$$F_1 = q.E \qquad \dots\dots\dots\dots\dots\dots\dots\dots\dots\dots (1.3)$$

Similarly, F_2 is the force experienced by ions in reverse direction which works to restore the initial equilibrium state (dipoles are assumed to act like springs having spring constant k) is expressed as

$$F_2 = k.E \qquad \dots\dots\dots\dots\dots\dots\dots\dots\dots\dots (1.4)$$

This constant k could be related to elastic modulus Y, and can be written as

$$k = Y.d_o \qquad \dots\dots\dots\dots\dots\dots\dots\dots\dots\dots (1.5)$$

In case of equilibrium, we have $F_1 = F_2$ and by relating equations, we find the estimated value of d as given below

$$d = \frac{q.E}{Y.d_o} \qquad \dots\dots\dots\dots\dots\dots\dots\dots\dots\dots (1.6)$$

So, the induced dipole moment for these ionic solids will be

$$\mu = q.d = \frac{q^2.E}{Y.d_o} = \alpha_i E \dots\dots\dots\dots\dots\dots\dots\dots\dots\dots\dots (1.7)$$

Where α_i is polarizability constant known as ionic polarizability. Hence the total polarization P can be expressed as

$$P = N.\mu = \frac{N.q^2.E}{Y.d_o} \qquad \dots\dots\dots\dots\dots\dots\dots\dots\dots\dots (1.8)$$

Where N is the density of dipoles per unit volume. It should be noted that the electric field E is considered parallel to the crystallographic axis and if this is not so, then we will take component of dipole moment in the field direction before adding them.

These calculations of ionic polarization are very rough and might be more complex for many ionic solids particularly in case of ions that haven't same charges i.e. CaF_2. Some ionic materials with their corresponding values of dielectric constant are listed in Table 1.2 [40].

18

Table 1.1: Values of dielectric permittivity of some materials

Material	Permittivity	Material	Permittivity
ZnO	4.6	MgO	3.0
ZnS	5.1	CdS	5.2
ZnSe	5.8	BeO	3.0
CdSe	7.0		

1.9.4 Dipolar/orientation polarization

In dipolar materials, an ionic bond is formed between two molecules by sharing their valence electrons, which causes dipole moment due to disparity in charge distribution and is equal to the product of sharing electrons and their interatomic spacings. In the absence of an external field, these induced dipoles are oriented randomly so that there is no net polarization. With the application of an external field, these dipoles orient themselves in the field direction and such phenomenon is known as orientation or dipolar polarization as shown in Fig. 1.19.
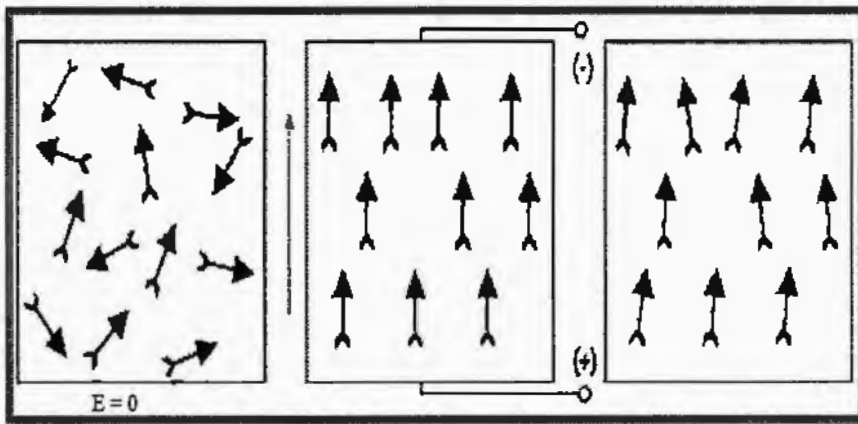
Fig. 1.19: Effect of electric field on dipole orientation [41].

In order to find a mathematical expression for orientation polarizability, we have to calculate net dipole moment and number of dipoles in material under investigation. Hence,

$$< \mu > = \frac{\mu}{N} \qquad \dots \dots \dots \dots \dots \dots \dots \dots \dots \dots \dots (1.9)$$

Hence, the relation for average polarization P will be

$$P = N \frac{\mu^2 E}{3 k_B T} \qquad \dots \dots \dots \dots \dots \dots \dots \dots \dots \dots (1.10)$$

At very low temperature and high applied field, all the dipoles will align parallel to the field direction and hence the total dipole moment will become equal to the theoretically calculated dipole moments [42].

1.9.5 Interfacial/space charge polarization

In dielectric materials, interfacial/space charge polarization exist due to the existence of charge carriers which could drift through a distance within the bulk of material by ionic conduction, hopping or diffusion, etc. This produces a macroscopic field alteration, observed in the form of an increase in sample capacitance to the observer and could be identical to the real increase of permittivity. Generally, this sort of polarization can he classified into two types i.e. interfacial polarization and hopping polarization. The localized charges (i.e. holes and electrons or ions and vacancies) in dielectric materials can produce hopping polarization by stepping from one site to another site. Similarly, with the application of an electric field, the separation of negative and positive charges creates an interfacial polarization. Usually, this happens at the grain boundaries or any other interface such as electrode material interface. This phenomenon is shown in Fig. 1.20.
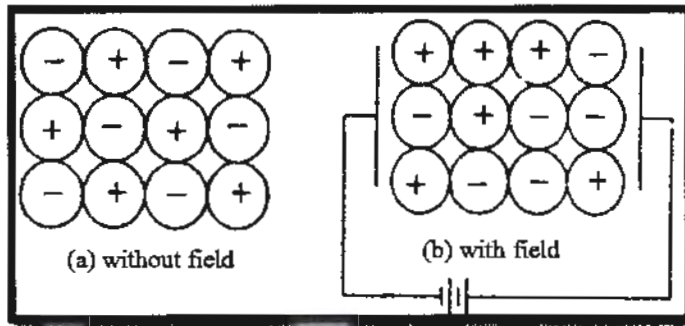
Fig. 1.20: Space charge/interfacial polarization [43].

By definition, atomic polarization is always there and any other mechanism would be counted as an addition. The mathematical analysis of the first three mechanisms is

straightforward and easy to handle, while that of interfacial polarization is too much difficult to quantify.

Qualitatively, we observed that in all of the above mechanisms, the displaced entities have different masses. The masses are getting smaller from dipolar to electronics to ionic polarization. It has a direct relation with the applied field frequency as shown in Fig. 1.21. Naturally, we can say that the particular entity with heavier mass will take more time in displacing. Typically, the atomic polarization persists in frequency range of 10^{13} to 10^{15} Hz and is the fastest polarization. The ionic polarization is a slow process and exists in frequency range of 10^9 to 10^{13} Hz while the dipolar polarization occurs where the moment of molecules are involved below 10^9 Hz. The space charge/interfacial polarization occurs at very low frequencies i.e. below 10 Hz [44].
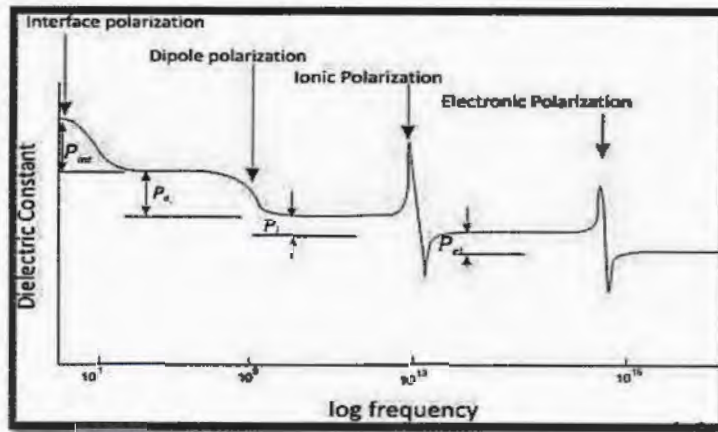
Fig. 1.21: Frequency dependence of different polarization mechanisms for dielectric material [45].

1.10 Classification of dielectric materials

On the basis of polarization mechanism, these materials are classified into two main groups: linear dielectric materials which may be further divided into three classes and non-linear dielectric materials.

1.10.1 Linear dielectric materials

Those materials which exhibit a linear relationship between polarization and applied field are known as linear dielectrics. These materials polarize when subjected to an

21

electric field and depolarize on the removal of external field. On the basis of their nature of polarization, these materials are grouped as follows:

1.10.1.1 Non-polar dielectrics

In this class of materials, an external electric field causes the elastic displacement of electron clouds (mainly that of valence electrons) and produces only the electronic polarization. Generally, such materials are referred to as elemental materials.

1.10.1.2 Polar dielectrics

In this class of materials, an external electric field not only induces the elastic displacement of electron clouds but also cases the displacement of their relative positions. Such type of materials possesses both the ionic and electronic polarizations. These materials may be composed of molecules and each molecule is made of more than one kind of atoms without permanent dipole moment. Ionic crystals are the examples of these materials and the net polarizability is the algebraic sum of both the electronic and ionic polarizabilities.

$$\alpha = \alpha_e + \alpha_i \qquad \text{............................(1.11)}$$

1.10.1.3 Dipolar dielectrics

These materials have all three fundamental polarizations i.e. ionic, electronic and orientation. So, the net polarizability is the sum of all the three kinds of polarizabilities.

$$\alpha = \alpha_e + \alpha_i + \alpha_d \qquad \text{..........................(1.12)}$$

Those materials, where the molecules possess permanent dipole moments are consider to this class of materials [46]. Its examples are water, methyl alcohol etc.

1.10.2   Non-linear dielectric materials

Those materials which are spontaneously polarized even by the absence of an external electric field are counted into non-linear dielectric materials. The crystal structure of these materials is responsible for the spontaneous polarization. The absence of center of symmetry is the necessary condition for non-linear dielectrics. Out of 32 crystal classes, only 11 have center of symmetry and don't possesses spontaneous polarization. In the remaining crystal classes, 20 are piezoelectric (i.e. they become polarized when subjected

to an external stress). Ten out of 20 piezoelectric crystals possess pyroelectric effect and their polarization is temperature dependent.

1.11   Research objectives

- To use simple and cost-effective synthesis technique i.e. sol-gel for the preparation of $Ni_{1-x}Mg_xCr_2O_4$ ($x = 0.0, 0.2, 0.4, 0.6, 0.8$ & 1.0) nanoparticles samples.
- Structural analysis by using XRD and TEM.
- Optical properties by using FTIR.
- Frequency dependent dielectric analysis.
- Magnetic properties by using (SQUID) magnetometer.

Chapter 2

Literature Review

2.1 Literature review

The general formula of spinel's structures is AB_2O_4 where A and B are divalent and trivalent cations, respectively and has a space group Fd3m[32]. This types of structure attracted much attraction due to there tremendous application in the different field of study. The properties of spinels structure are effected by the arrangements and the nature of ions in spinel structure. $NiCr_2O_4$ can be used as an important catalyst for a number of industrial applications [47]. Due to a number of potential applications and magnetic properties chromium based spinel compound ACr_2O_4 pull a lot of attraction in this type of spinel compound $A=Cu^{2+}$, Fe^{2+}, Ni^{2+}, $Co^{2+,}$ and Mn^{2+}. In normal spinel nickel chromite ($NiCr_2O_4$), Ni^{2+} occupy A-sites and Cr^{3+} live on the B sites. Also various studies are carried out to study the thermodynamic properties of chromium based spinal structures both in materials science and also in earth. $NiCr_2O_4$ is also used in the gas sensors. Nickel chromite also used as a catalyst, pigment, magnetic material, semiconductor, sensors [48]. Numbers of the method are reported for the synthesis of nickel chromite involves combustion reaction, spray-drying , sol-gel combustion, co-precipitation thermal treatment and hydro thermal [49]. The sol-gel method has the benefit including fine crystalline with small size distribution, shape, and size control, economical and easy route, consistent and high efficiency[50]. $NiCr_2O_4$ and $CoCr_2O_4$, have the normal spinel structure (AB_2O_4), in which the A^{2+} cations, (Ni^{2+} (3d8) or Co^{2+} (3d7)) are in tetrahedral oxygen coordination and the Cr^{3+} cations reside on the octahedral (B) site [51].

Enhessari *et al* [52] successfully synthesized $NiCr_2O_4$ nanoparticles via a sol-gel method. The X-ray diffraction analysis confirmed the formation of spinel structure without any minor phase and by using Debye scherrer's formula, obtained average crystallite size was 24 nm. In the FTIR study, two absorption bands observed below 1000 cm^{-1} at 616 and 495 cm^{-1} confirm the formation of metal oxygen (Cr-O and Ni-O) bonds. Moreover, a sharp absorption at about 883cm^{-1} indicates

the (Ni-Cr) vibrational frequencies. The value of magnetization obtained ~0.2emu/g in 8 kOe applied magnetic field at 25°C. This showed that the paramagnetic behavior of $NiCr_2O_4$ nanoparticles; however, the $NiCr_2O_4$ in bulk is ferromagnetic materials. Magnetic, optical band gap properties showed that the ultimate nanoparticles are magnetically and optically active. The optical band gap of 1.7eV confirmed the semiconductor nature of the material. This showed that this material could be used in modern electronic devices.

Ahu Bakar *et al.* [53] synthesized the nickel chromite nanoparticles and study the calcination temperatures effect on obtained materials. The final Nano particles were carefully characterized by different techniques. The FTIR study revealed two metals–oxygen bonds for Cr–O around 470 cm^{-1} and Ni–O at 600 cm^{-1}. The Nano particle obtained have average particle size of 7-64nm calculated from TEM (transmission electron micrographs) at calcination temperatures range from 550-850°C. The samples showed a paramagnetic nature at calcination temperatures of 750°C and 850°C with field value of 342.04 and 306.49 Oe with g factor of 1.92 and 2.15, respectively. The variation in these properties attributed to super exchange and dipole–dipole interaction. Only few papers reported magnetic studies of $NiCr_2O_4$ in detailed.

Barman *et al.* [54] synthesized nickel chromite nanoparticles from a solution constitute of chromium nitrate, polyvinyl pyrrolidone, nickel nitrate, and distilled water followed by grinding, baked and oxidation at different temperatures. They studied turning effect and exchange interaction of $NiCr_2O_4$ nanoparticles which were studied by using sol–gel synthesis method. They studied that at $T_C = 73$ K the sample gave ferrimagnetic transition. The sample displayed exchange bias phenomenon which were explained on the basis of anisotropic interactions among the antiferromagnetic and ferrimagnetic component. As temperature increases exchange bias field decay, exponentially and also showed the existence of training effect.

Patk *et al.* [55] synthesized the $NiCr_2O_4$ nanoparticle by co-precipitation method and found that these particles showed both tetragonal and cubic phases at temperature of about 1000°C and 800°C, respectively. John–Teller distortion at 800°C is also much lowered and about 243 K in the temperature dependent X-ray diffraction studies. The magnetic study of $NiCr_2O_4$ nanoparticles which were synthesized at 800°C is totally different from the magnetic properties of

the bulk $NiCr_2O_4$. They also observed the existence of Cr_2O_3 impurity in the sample in the form of additional band at 638 and 665 cm^{-1}.

Liu *et al.* [56] synthesized nitrogen doped $NiCr_2O_4$ by solid state reaction method by rising the temperature of high purity NiO and Cr_2O_3 mixture in air and also studied the effect of anion doping on magnetic and structural properties. The phase transition of $NiCr_2O_4$ is caused by the Jahn–Teller effect of the Ni^{2+} cations on the tetrahedral site. The structural and magnetic transition is also observed in magnetic measurements of nitrogen (N) doped $NiCr_2O_4$. Atomic force microscopy showed that transitions are detected at T_S = 22 K and 23 K at temperature for 873 K and 773 K respectively. They also studied that doping lower the transition values as compared to the bulk value. Their material also showed a permanent magnet behavior in a temperature range of T ~ 80 –350 K which is proved by M-H loop. They reported that doping had increased the frustration and decreased the correlation length of $NiCr_2O_4$. They also investigated that for the synthesis of metal oxides thermal method had many advantages such as economical, environmentally friendly and easy to control.

Mantlikova *et al.* [57] recently studied $NiCr_2O_4$/SiO_2 nanocomposites and $NiCr_2O_4$ fine powder and observed that there is no change in magnetic phase transition T_C and T_S even the crystallite goes to 10.6 nm. They studied that the surface spin effects reduced the magnetization. The temperature-dependent studies of phonon are very useful to study the spin field phonon and spin-phonon interaction in ferroelectric and multiferroic materials. In $CoCr_2O_4$ no phase transition is observed but $NiCr_2O_4$ go through a tetragonal phase transition because of the john-teller distortion. They studied that Below 320 K, the symmetry of $NiCr_2O_4$ lowers to tetragonal, whereas $CoCr_2O_4$ remains cubic down to 11 K. They also studied that both $CoCr_2O_4$ and $NiCr_2O_4$ compounds undergo ferrimagnetic ordering at T_N 95 K and 70 K, respectively. A structural phase transition was also found at a lower temperature about 65 K, which is somewhat different from the magnetic transition temperature.

Rudolf *et al.* [58] studied the spin phonon properties of antiferromagnetic spinel chromium structure very profoundly. The spin phonon coupling showed splitting of phonon mode when it go through magnetically phases transition. They studied that pressure studies of spinels structures showed two sorts of high-pressure behavior one goes through a transformation from spinel arraignment to single poly-morph another split up to a substance of organic oxides.

Terada *et al.* [59] reported the polycrystalline infrared spectrum in which they observed only two IR bands. They studied IR spectra of some spinel chromite's $NiCr_2O_4$ and $FeCr_2O_4$ in the region from 265 to 4000 cm^{-1} with the help of spectrometer and observed two strong and one weak absorption bond in this region. They studied that v_1 band for chromite and ferrites are almost same but v_2 band of chromite is much higher than that of ferrites. They also studied that the difference arise in v2 band is due to the formation of a new band in chromites and its frequency is higher than the metal ions band in isotropic field.

Honeybourne *et al.* [60] studied the sensing properties of synthesized $NiCr_2O_4$, $CuCr_2O_4$ and $ZnCr_2O_4$ nanoparticles. X-ray diffraction confirmed their structures. They also doped Mg and Li and studied that doping of Mg and Li altered the spinel property of gas sensing. They studied that $NiCr_2O_4$ is useful as a catalytic material. They also investigated that the chromium is mostly found in interior of the earth in mineral state has basic application in applied physics and material science.

Mufti *et al.* [61] synthesized the $NiCr_2O_4$ by using solid-state reaction method and studied the magneto coupling in frustrated spin system of spinel $NiCr_2O_4$. They studied the dielectric anomalies on the canted structure of $NiCr_2O_4$. Due to uses in material science and geology chromite are considered as important spinels. They investigated that at lower temperature some chromite showed ferrimagnets behavior and $CoCr_2O_4$ showed multiferroic arrangement below the temperature of 26 K.

Crottaz *et al.* [62] synthesized the $NiCr_2O_4$ by flux decomposition method and used the X-ray powder diffraction to measure the cell parameters. The crystal is undergoing through phase transition at 320 K. The transitions are reported at the temperature of 320 K (tetragonal phase transition) has been generally studied and is normally explicate as caused by a John teller distortion of ions and other magnetic transition at temperature ranging from 60 to 80 K.

Chapter 3

Synthesis and Characterization Techniques

In this chapter, I will discuss about the preparation and characterization of the material under test which is Mg doped $NiCr_2O_4$ (x=0, 0.2, 0.4, 0.6 ,0.8 and 1) nanoparticles.

3.1   Synthesis of nanoparticles

For the synthesis of nanoparticles, we mostly use two approaches

- Top down technique
- Bottom up technique

3.1.1 Bottom up technique

The synthesis method in which large numbers of atoms or molecules combine at the nano-scale to form nanoparticles is known as bottom up technique. The most common bottom up synthesis approaches are as under: -

- Chemical vapor deposition
- Co-precipitation
- Physical vapor deposition
- Sol-gel method
- Hydrothermal technique
- Electrochemical deposition
- Precursor method

3.1.2 Top down technique

In this technique, a bulk material is divided up to the atomic scale to form nanoparticles is known as top down technique. Top down synthesis approaches include

- Ball milling
- Lithography

- Laser ablation

3.2   Fabrication of chromite sample

I used sol-gel method for the synthesis of $NiCr_2O_4$ nanoparticles which is basically a chemical synthesis method. In this method, there is the formation of an oxide network through molecular precursors throughout the liquid. This method is the combination of two terms the sol and the gel as shown in Fig. 3.1. Sol is a colloidal holdup of solid particles in a solvent while gel consists of three-dimensional network of agglomerated particles. The main idea behind this technique is to dissolve solid particles in a liquid in order to mix them with other particle and then bring them again as a solid to form new compounds.
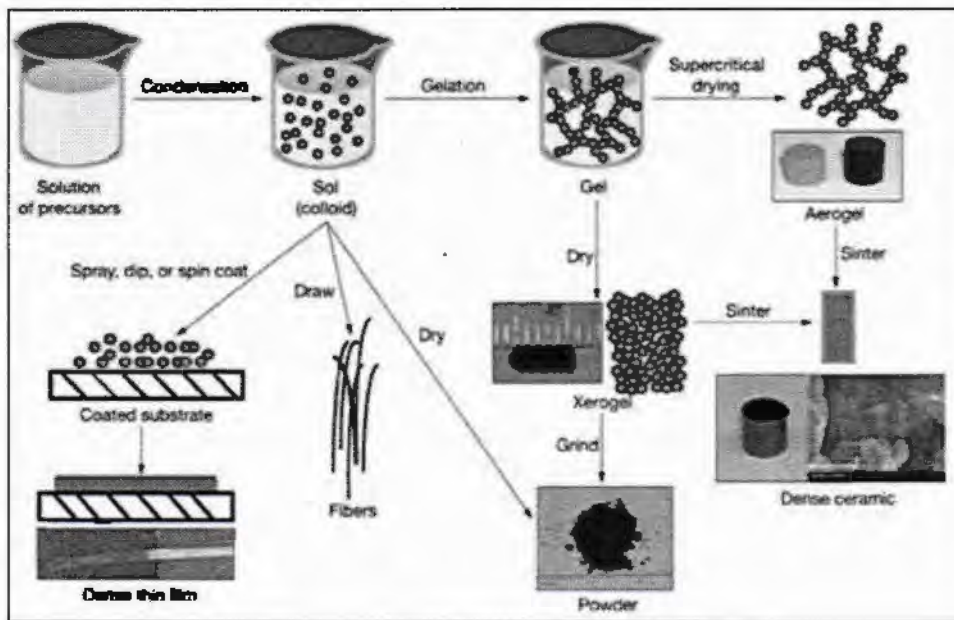
Fig. 3.1: Sol-gel synthesis process [63].

The key advantages of using this technique are:

- Multi-components compounds can he made very easily by mixing the solutions of different compounds and their stoichiometry can be controlled.
- Results in high purity products.
- Low temperature sintering is required because of the formation of small particles.
- Enable mixing at atomic level.
- Gelation process minimize the problem of co-precipitation.

29

- Materials can be shaped easily into complex geometries.

To prepare Mg doped $Mg_xNi_{1-x}Cr_2O_4$ (x=0, 0.2, 0.4, 0.6, 0.8 and 1) nanoparticle correct quantity of materials were weighted through the analytical electronic balance. We mostly used the materials in nitrates form which were gained from Sigma Aldrich.

All nitrates were ACS reagent with purity level of higher than 99%. First, we took the stoichiometric ratios of the Mg, Ni and Cr nitrates and made a solution with the help of ethanol. Made another solution of citric acid dissolved in distilled water. Then mixed these both solutions with the help of magnetic stirrer without heating and continuously stir it until both are dissolved completely. Then I added the ammonia in it to set the value of pH at 5. After adjusting the pH value, start heating the desired solution at 70°C. After 45-50 minutes, a gel like material is formed. When gel is completely formed at this point, stirring process is stopped. Then placed this gel for drying in an electric oven for overnight and obtained a glossy blackish material. The precursor was obtained in the form of powder with the help of mortar. After this, annealed the sample in a furnace at 900°C for 2h to get the desired $Mg_xNi_{1-x}Cr_2O_4$ nanoparticles of different Mg concentration of x (x=0, 0.2, 0.4, 0.6, 0.8, and 1). Flow chart of synthesis of $Mg_xNi_{1-x}Cr_2O_4$ nanoparticles is shown in Fig. 3.2.
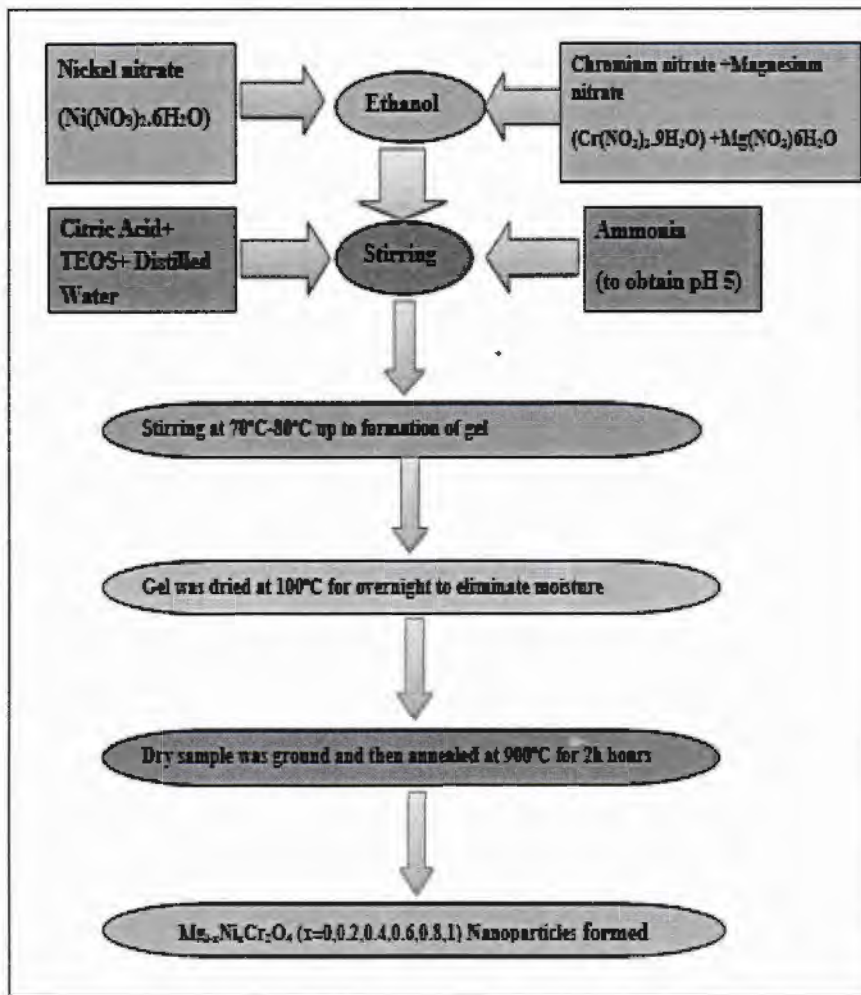
Fig. 3.2: Flow chart of synthesis of $Mg_xNi_{1-x}Cr_2O_4$ nanoparticles.

3.3   Pellet formation

For Impedance or dielectric measurements, we require pellets which are cylindrical form have a plane surface. Pellet of 10 to 12 mm diameter were prepared. These pellets are formed in a hydraulic press by simply compressing the powder which is form of the bulk material. The Thickness of the pellets was maintained in between 1 mm to 1.5 mm.

3.4   Characterization techniques

To study the desired properties of the material I have performed some of the experiments using the following techniques.

- X-ray diffraction (XRD)
- Transmission electron microscopy(TEM)
- Fourier transform infrared (FTIR) spectroscopy
- SQUID (superconducting quantum interference device) measurement
- Dielectric measurements (6500B Wayne-Kerr Impedance Analyzer).

3.4.1 X-ray diffraction

X-ray diffraction is a non-destructive and versatile experimental technique for identification of the different phases of material (crystalline). This technique also provides the information about the crystallite size, unit cell dimensions and locate different dislocation or imperfection in the material and we can also find the interatomic remoteness up to 10^{-10} m [64].

X-rays were discovered by Wilhelm Conrad Rontgen in 1895 also called Rontgen radiations. X-rays are electromagnetic radiations with high penetrating power than light rays, having high frequencies and smaller wavelength in the range of 3×10^{16} to 3×10^{19} Hz and 0.01 to 10 nm, respectively. The corresponding energies of X-rays ranges from 100 eV to 100 keV. Based on penetration power, X-rays are classified into two categories. X-rays having wavelength of the order of 10 to 0.10 nm or energy from 0.10 keV to 10 keV are known as soft X-rays while those having wavelength of the order of 0.10 to 0.01 nm or energy from 10 keV to 100 keV are known as hard X-rays [65]. Fig. 3.3 shows the schematic diagram of production of X-rays.
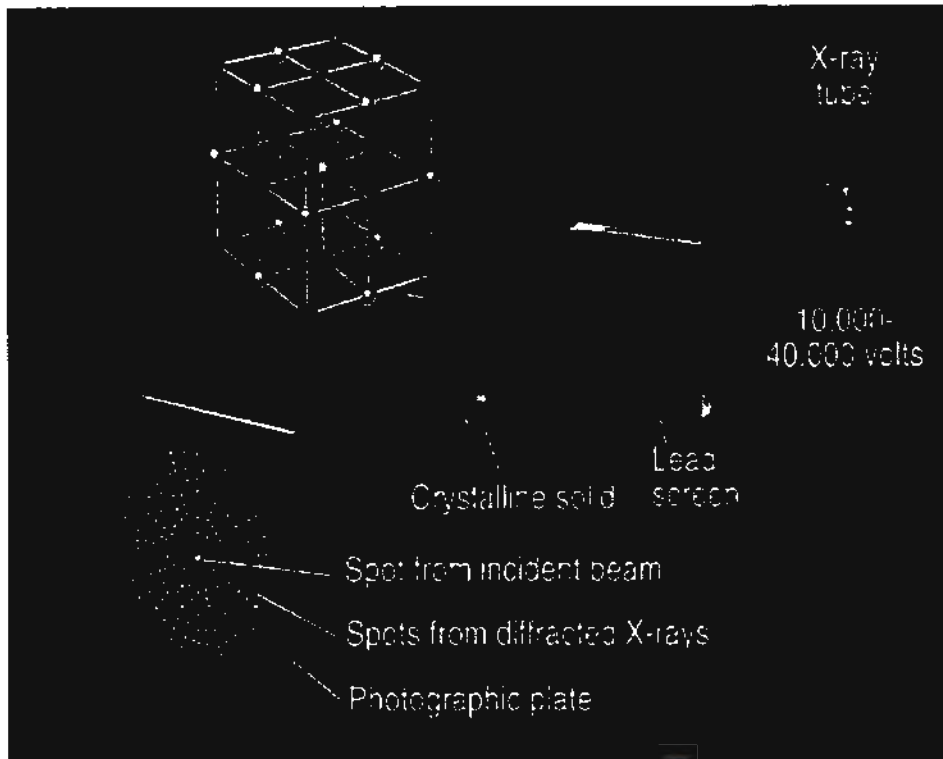
Fig. 3.3: XRD instrumentation [66]

3.4.1.1   Bragg's law

The fundamental of the X-rays diffraction is Bragg's law which was given by W.H Braggs in 1913. Bragg's law explains that when X-rays are falls on a crystal then crystals atoms reflects it's at a certain angle(θ) while acting as a mirror as shown in Fig. 3.4.

The diffraction phenomena arise only when the scattered X-rays have a path difference of integral multiple of the wavelength of the incident X-ray which we called a constructive interference. If the path difference of the scattered X-ray is half of integral multiple of the wavelength of the incident X-rays then its said to be the destructive interference. Formula of Bragg's law is given below:

$$2d\sin\theta = n\lambda \qquad \text{................................} (3.1)$$

Here 'n' is reflection order have an integral value. The diffraction occurs only at definite angle and if the ratio of $n\lambda$ to $2d$ is less then unity then only Bragg's satisfy.

33

$$2d\,sin\theta = n\,\lambda$$
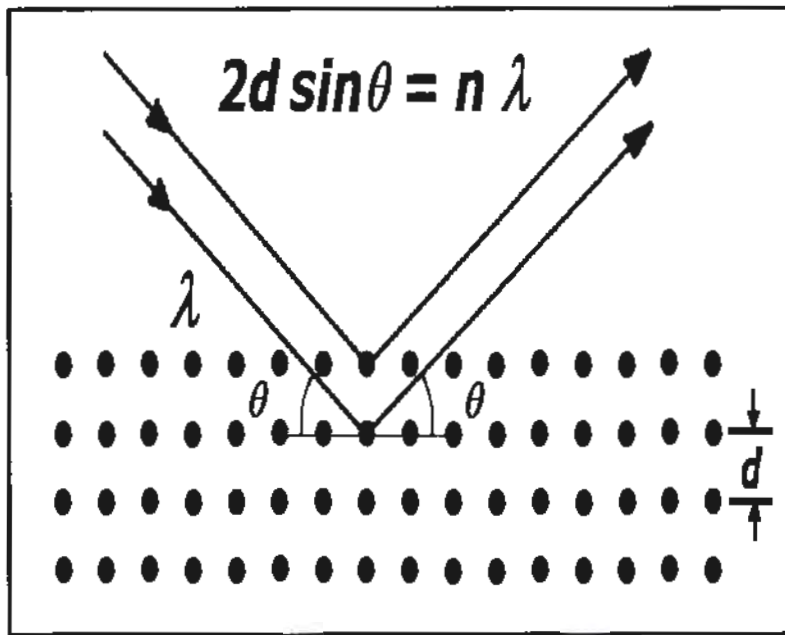
Fig. 3.4: Brags law [67].

3.4.2 Methods of X-ray diffraction

Different methods of diffraction are given below.

- Laue method
- Powder method
- Rotating crystal method

3.4.2.1   Laue method

For determination of symmetry and orientation of the single crystal a method or simply to observed the crystallographic axes and structural analysis of a single crystal we use Laue method is used known as Laue's diffraction method. In this method X-ray beam to be fall on a single crystal which only select some wave lengths and satisfies Bragg's law. The beam is observed on photographic film as a spot. Depending on the position of crystal, source and photographic film two distinction in Laue's method are observed. If the film is located behind the crystal and diffracted beam is recorded in the forward direction, this case in known as transmission Laue method. If the film is

placed between the X-ray source and crystal its known as back Laue's method [69]. The schematic diagram of Transmission and Back reflection laue method is given in Figure 3.7.
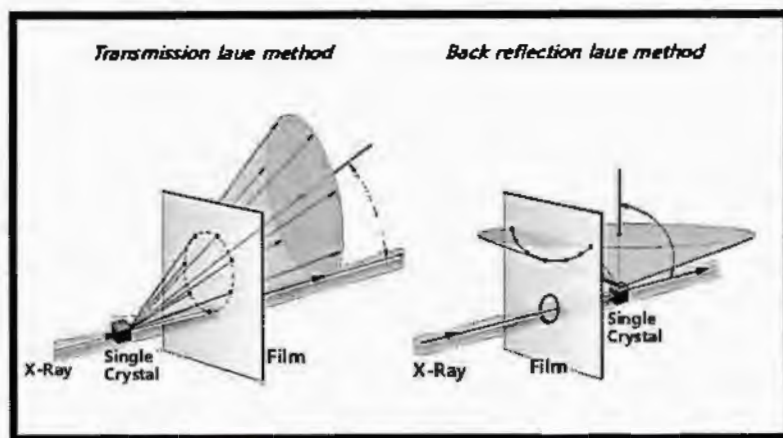
Fig. 3.5: Laue method for X-ray diffraction [68].

3.4.2.2 Powder method

The Powder diffraction technique offer information about construction of crystalline structure and about dimensions of unit cell. The crystallites are randomly oriented in many directions in powder form and the incident beam interacts with it and produced diffraction. Due to unique set of D-spacing of crystalline phase the material can be easily recognized [69]. The schematic diagram of powder method is shown below Fig. 3.6.
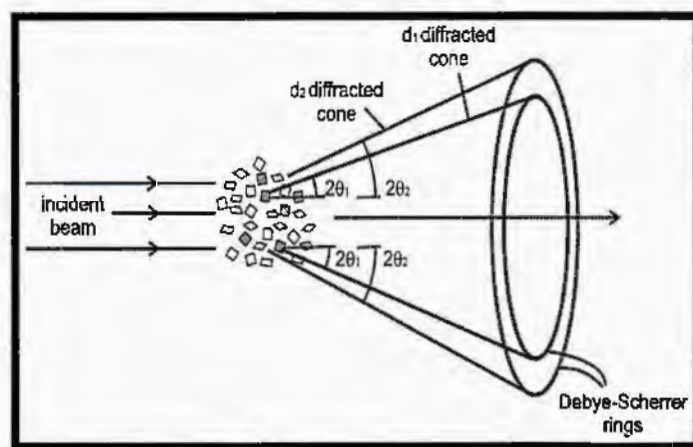
Fig. 3.6: Formation of a diffracted cone of radiations in powder method [70].

3.4.2.3 Rotating crystal method

In this method, a single crystal arranged in such a way that its one axis is normal to X-ray beam (monochromatic). The rotational motion of this beam around an axis used to investigate the crystallographic direction of lattice as shown in Fig. 3.7.
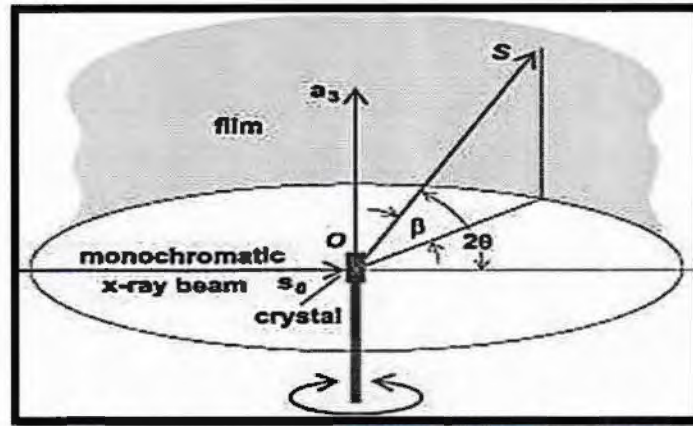
Fig. 3.7: X-ray diffraction through rotating crystal method [71].

3.5   Transmission electron microscopy

Transmission Electron Microscopy is an imaging technique in which broaden version seen when a beam of electrons passed through on a sample (specimen). Albert Prebus and James hillier jointly built first transmission electron microscopy in 1938 by following the concept which were given by the Max Knoll [72]. Transmission Electron Microscopy is good technique to produce image of simple with high resolution. The basic principle on which TEM is based upon is Lorentz force. A TEM consists of electromagnetic lenses, fluorescent screen, electron gun, stage. The electrons are produced by electron source then passing through a serious of electromagnets which are basically focus the electron beam on a sample and the final image is produced on the florescent screen. The image produced on the fluorescent screen depends upon the thickness of the sample.

The schematic diagram of TEM is shown in Fig. 3.8. Different images and contrast are produced by the direct and diffracted electrons. This technique is greatly work for perfect crystal prominent contrast. When diffracted and direct electron strikes on the sample they formed a phase contrast. Due to phase, bright and dark images formed in TEM.
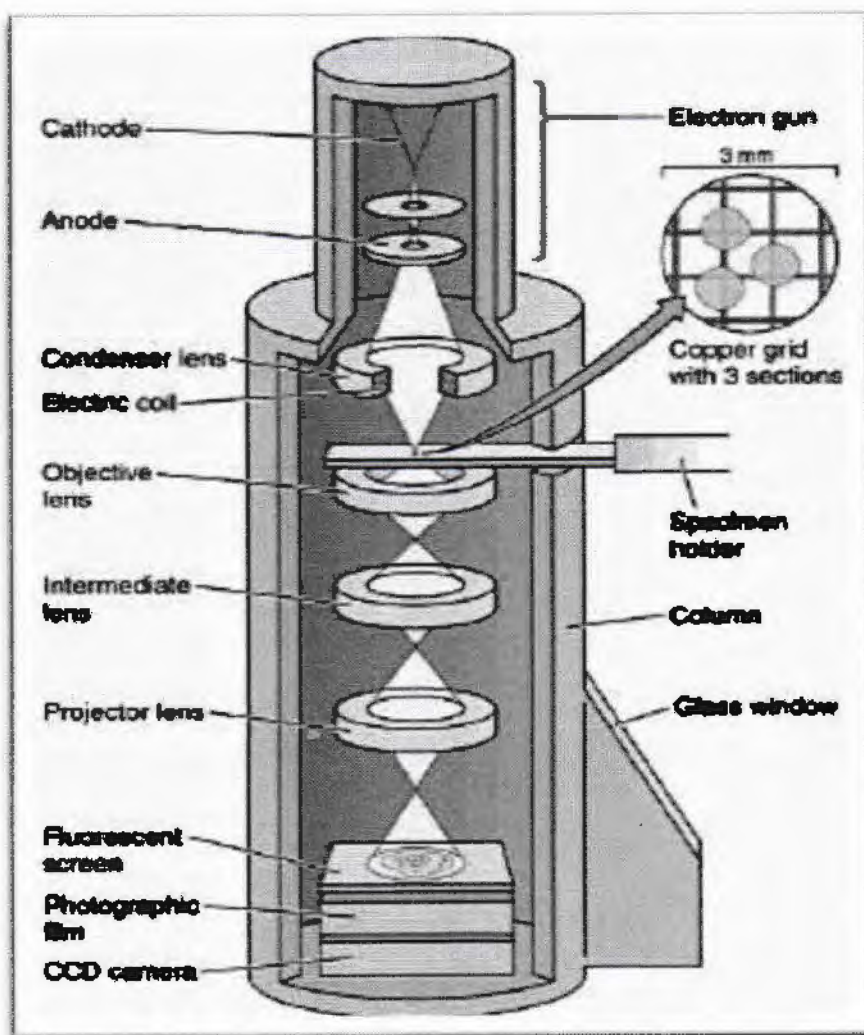
Fig. 3.8: Systematic diagram of TEM [73]

3.6   Fourier transform infrared (FTIR) spectroscopy

FTIR is an infrared spectroscopy in which IR radiation are fall on a sample. A part of IR radiation captivated by sample and other part is transmitted. As a result, spectrum is obtained which is the thumb impression of the sample because no two samples have a same molecular spectrum that makes FTIR useful for different type of materials analysis. Therefore we can say that FTIR provides information for identification of materials, quality of sample and determination of different component in a material compound. We can easily identify the various types of materials with the help of their different spectrum images. As FTIR is a non-destructive technique

so it is favored on other dispersive IR analysis, very high speed gives a scan in every second, greater optical throughput and mechanically simple technique. Fourier Transform Infrared spectrometry works on the principle of simple optical device called Michelson interferometer. Fig. 3.9 shows the construction and working of Michelson interferometer.

A Michelson Interferometer
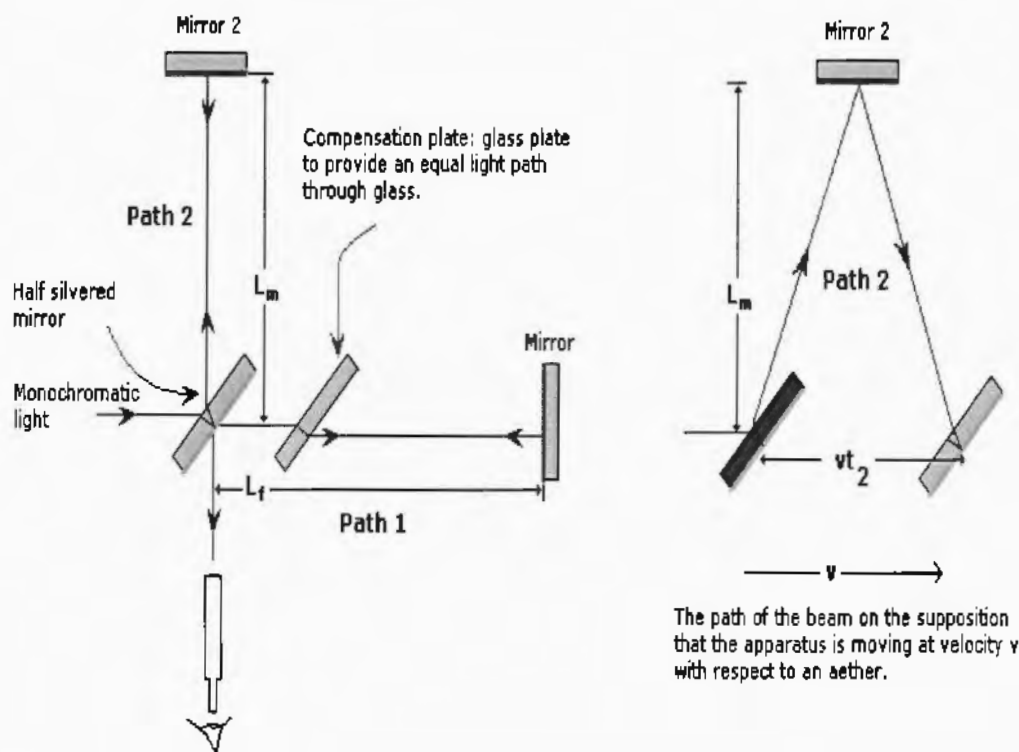
Fig. 3.9: Michelson interferometer working [74]

A well-known technique known as Fourier transformation is used for this purpose which can be performed on the computer which gives desired spectral information to the user. The normal instrumental setup is as follows:

- **Source:** The glowing black body emitted infrared rays; this beam is passing through an aperture which control the energy beam fall on the sample.

- **The Interferometer:** In the interferometer, the beam "encoding" is take place then the resulting signal exists from the interferometer.

- **The Sample.** In this step, the beams enter in the compartment of sample where it reflected or transmitted off from the sample surface depends upon the type of analysis being done. Here certain frequencies absorbed by the sample which can be used to identify the sample.

- **Detector:** Then this ray is passing through the detector, which is specially designed for interferogram signal measurements.

- **The Computer:** The obtained signal digitized and the ultimate infrared spectrum is attained to the user for any more explanation.

3.7   Superconducting quantum interference device (SQUID) magnetometer

SQUID is a magnetometer works on the principle of Josephson junctions which is used to measure the magnetic field and it comprises of superconducting loops. Working of SQUID as Josephson effect is shown in Fig. 3.10.
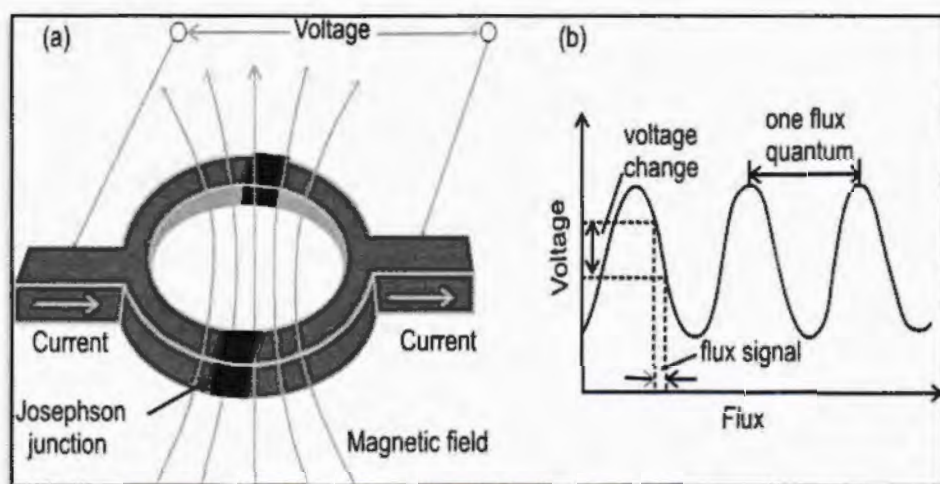
Fig. 3. 10: Josephson effect [75].

SQUID magnetometer is constructed in such a way that it measures the extremely small magnetic field. It is very sensitive device which calculate change in one flux quantum. SQUID is also used for measurements of magnetization of a single crystal in temperature of 4.2-400 K at very low and high magnetic fields. The applied field value of SQUID is varying from 10^{-15} T to a max value of ± 7 T due to quantized state of the ring and joseph junction's non-liner behavior. Some systems are more sensitive than squid like (MPMS) magnetic property measurement system

but not measure the magnetic field value directly. The output voltage and squid have a proportionality.
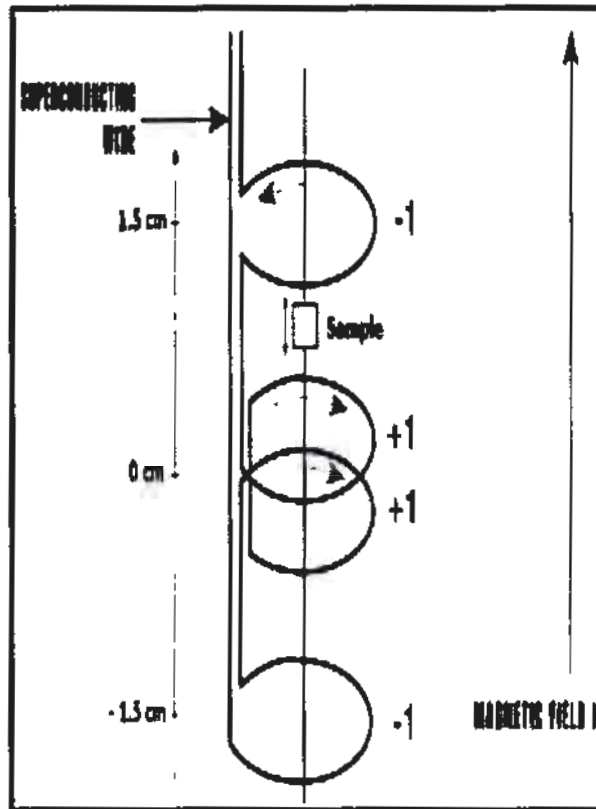
Fig. 3.11: Pick up coil of SQUID [76].

Pick up coil of SQUID is shown in Fig. 3.11. A superconducting coil placed at magnet's center move the sample up and down between these coils and for accurate measurements, we place the sample up to 3 cm, which is the center of the upper and bottom coil. SQUID changes current into voltage and it is related to magnetic moment.

3.8 Dielectric measurements

The frequency dependent dielectric measurements of $Mg_xNi_{1-x}Cr_2O_4$ ($x = 0.0$, 0.2, 0.4, 0.8 & 1) nanoparticles samples, in frequency range of 100 Hz to 5 MHz, were carried out by using Wayer-Kerr 6500B impedance analyzer. Dielectric measurements are done for the analysis of electrical properties. Dielectric materials are very important for technological applications because

they possess electrical polarization. Dielectric constant can be calculated by using following formula:

$$\varepsilon' = \frac{Cd}{\varepsilon_o A} \quad\quad \dots\dots\dots\dots\dots\dots\dots\dots\dots\dots\dots (3.2)$$

In above formula, the free space permittivity is denoted by ε_o, C is the capacitance of pellet in parallel arrangement (unit of capacitance used is farad, pellet area is donated by A and d is the thickness of pellet. The formula used to calculate Dielectric loss is given bellow:

$$tan\delta = \frac{1}{2\pi f R_p C_p} \quad\quad \dots\dots\dots\dots\dots\dots\dots\dots\dots\dots\dots (3.3)$$

In above formula, f is the frequency, R_P is the resistance in parallel and C_P is the capacitance in parallel. Formula of loss factor is given below.

$$\varepsilon'' = \varepsilon' tan\delta \quad\quad \dots\dots\dots\dots\dots\dots\dots\dots\dots\dots\dots (3.4)$$

3.8.1 LCR meter or impedance analyzer

Impedance analyzer 6500B was used for the measurement of dielectric properties during experimental work as shown in Fig. 3.12. This provides very accurate dielectric measurements in different frequency ranges up to 5 M Hz. It shows accuracy of ± 0.05% which makes it very suitable for this purpose. Sample is placed between two metal plates in the form of pellets and frequency of desired range is applied. The properties are analyzed in that range of frequency and results are displayed on the screen in the form of parameters. Temperature dependent properties are also measured through this instrument. In that case, heater is used in which required temperature can be adjusted. The parameters which can be measured by this analyzer are Capacitance (C), Admittance (Y), Reactance (R), Inductance (I), Resistance (R), Impedance (Z), Susceptance (B), Quality factor (Q), Conductance (G), Dissipation factor (D) and phase angle (θ). Any two parameters can be measured simultaneously. Measured parameter's data can easily be stored in USB flash memory.
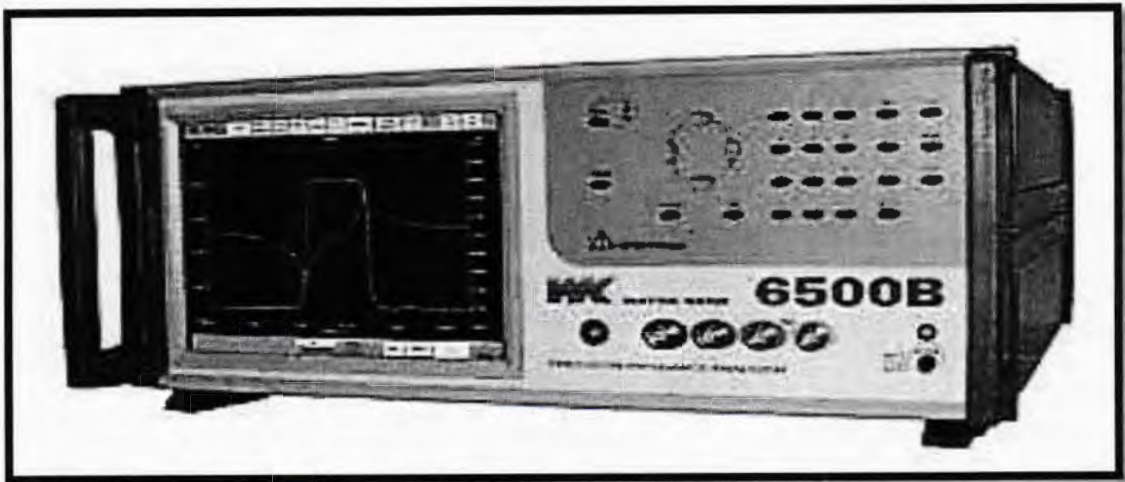
Fig. 3.12: 6500B series of precision impedance analyzer [77].

Chapter 4

Results and Discussion

A series of chromite samples having general formula $Mg_xNi_{1-x}Cr_2O_4$ (x=0, 0.2, 0.4, 0.6, 0.8 and1) was prepared via sol-gel method and were subjected to different characterization techniques to investigate their structural, dielectric, and magnetic properties. The structure of $Mg_xNi_{1-x}Cr_2O_4$ (x=0, 0.2, 0.4, 0.6, 0.8, and 1) samples were inspected from XRD. The magnetic measurements were done by SQUID magnetometer. FTIR spectroscopy was also done to study the different vibrational modes. The frequency dependent dielectric study was done by using Wayne-Kerr 6500 B Series Precision Impedance Analyzer in the range of 10 kHz to 10 MHz. The results obtained are discussed here in detail.

4.1   X-Ray diffraction

X-ray diffraction (XRD) technique was used for the structural analysis of all the prepared $Mg_xNi_{1-x}Cr_2O_4$ (x = 0, 0.2, 0.4, 0.6, 0.8 and 1) samples. X-ray diffraction analysis provides information about the phase formation, crystallite size, lattice parameter and crystalline nature of materials. Figure 4.1 shows the XRD patterns of $Mg_xNi_{1-x}Cr_2O_4$ (x=0, 0.2, 0.4, 0.6, 0.8 and 1) nanoparticles prepared by sol-gel method. All the samples exhibit spinel structure. In any diffraction pattern, the diffracted peaks describe the crystal structure, the lines positions provide information about the unit cell and the line intensities can be described the atomic positions. Higher peaks in XRD pattern describe that the diffraction takes place from those planes having greater concentration of lattice atoms. For sample when $x = 0.0$, the highest peak is found at 2θ value of 35.42° of miller indices (311). XRD pattern confirms the single phase, purity and crystalline nature of our prepared samples. It is clearly shown in Fig. 4.1 that Mg^{2+} doping did not affect pattern of XRD therefore no impurity peaks associated to any secondary phase were observed in these patterns.

43

For the sample x= 0, all the peaks are well matched with JCPD card # 23-432, which shows the formation of cubic spinel structure of $NiCr_2O_4$. The average particle size is calculated by using Debye-Scherrer's formula.

$$D_{hkl} = k\,\lambda/\beta\,Cos\theta_B \qquad \ldots\ldots\ldots\ldots\ldots\ldots\ldots\ldots\ldots\ldots\ldots (4.1)$$

Where,

λ = wavelength of Cu K_α used in X-ray diffraction

β = Full width at half maxima (FWHM) which is taken in radians

k = a dimensionless quantity called shape factor and is equal to 0.9

θ_B = Bragg's angle of diffraction

The average crystallite size is calculated in the range of 26 nm [53] for x=0.0. The average crystallite size of the particles shows an overall increasing trend with Mg concentration because $Mg(0.72^0A)$ which has larger ionic radius then $Ni(0.69^0A)$. The non-uniform trend of crystallite size depends upon the synthesis process.
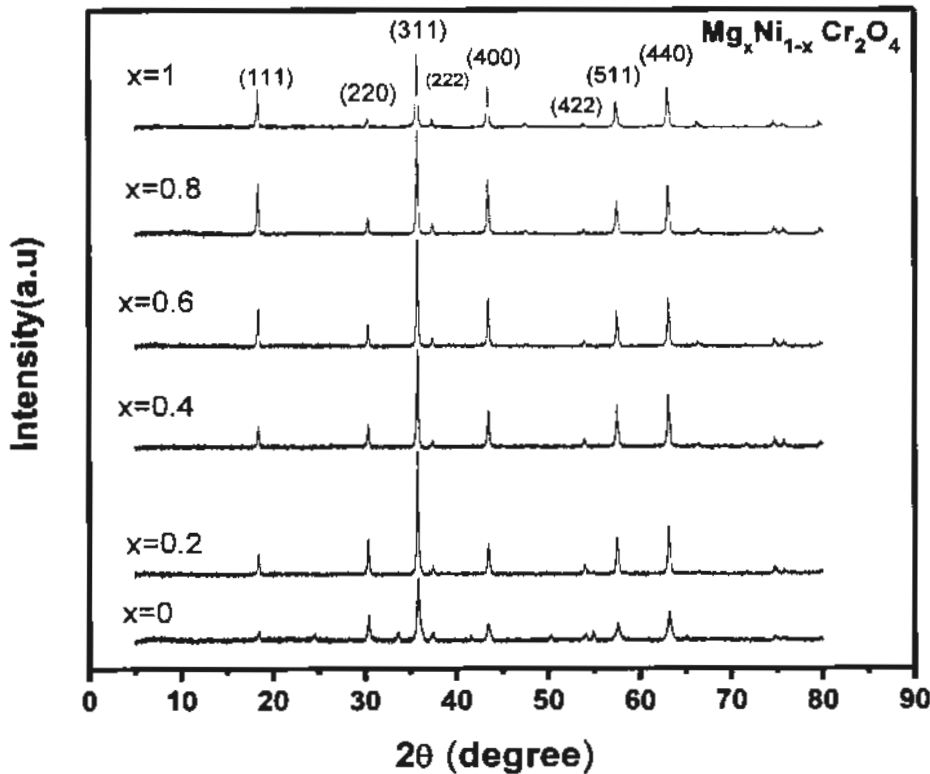
Fig. 4.1: XRD patterns of $Ni_{1-x}Mg_xCr_2O_4$ (x = 0, 0.2, 0.4, 0.6, 0.8 & 1) nanoparticles.

To calculate the lattice parameter we use Bragg's law,

$$2d \sin \theta = n\lambda \qquad \ldots \ldots \ldots \ldots \ldots \ldots \ldots \ldots \ldots \ldots \ldots \ldots \qquad (4.2)$$

The relationship between d-spacing and *hkl* values for a cubic system is also given as,

$$d_{hkl} = a/\sqrt{(h^2 + k^2 + l^2)} \qquad \ldots \ldots \ldots \ldots \ldots \ldots \ldots \ldots \ldots \ldots \ldots \ldots \ldots (4.3)$$

Where '*a*' is the lattice parameter. By putting Eq. 4.3 in Eq. 4.2 and re-arranging, we get,

$$a = \frac{\lambda\sqrt{(h^2 + k^2 + l^2)}}{2\sin\theta} \qquad \ldots \ldots \ldots \ldots \ldots \ldots \ldots \ldots \ldots \ldots \ldots \qquad (4.4)$$

Lattice parameter can be found by using the above relation 4.4. By putting values of λ, *hkl*, and their corresponding θ values, we can calculate the lattice constant of each individual peak. By taking average of all the calculated values of lattice constants, we obtained the actual value of lattice constant of *FCC* structure for all the samples.
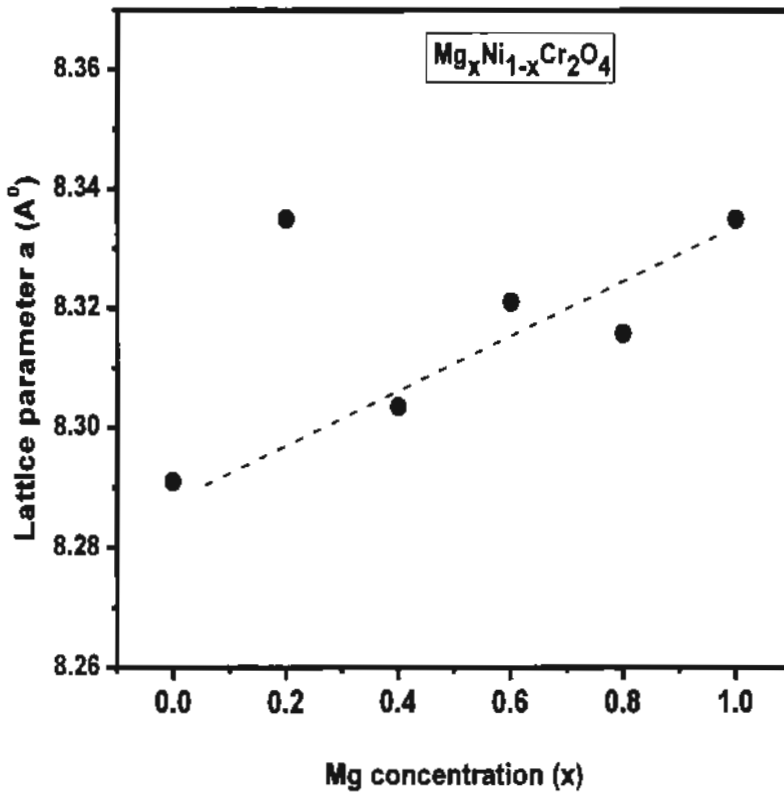
Fig. 4.2: Variation of lattice parameter with Mg concentration (x) of $Ni_{1-x}Mg_xCr_2O_4$ nanoparticles.

Figure 4.2 shows the variation in lattice parameter 'a' with Mg concentration for $Mg_xNi_{1-x}Cr_2O_4$ (x=0, 0.2, 0.4, 0.6, 0.8 and 1) nanoparticles. This increasing trend is due to larger ionic radius of Mg(0.72^0A) ion as compared to Ni(0.69^0A) ion but the subsequent increase may be attributed to various uncontrolled parameters (pH value, dopant's lattice preference and accumulation to an interstitial site etc.

Figure 4.3 shows the variation in average crystallite size with Mg concentration for $Mg_xNi_{1-x}Cr_2O_4$ (x=0, 0.2, 0.4, 0.6, 0.8 and 1) nanoparticles. The average particle size shows overall increasing trend with Mg concentration because the ionic radius of dopant Mg is larger than that of Ni on A site. As we replace a smaller ionic radius (Ni) with larger ionic radius Mg so as a result the average particle size increases with Mg doping on $NiCr_2O_4$ nanoparticles.

For both lattice parameter and average crystallite size, nanoparticles with x = 0.2 show maximum values.
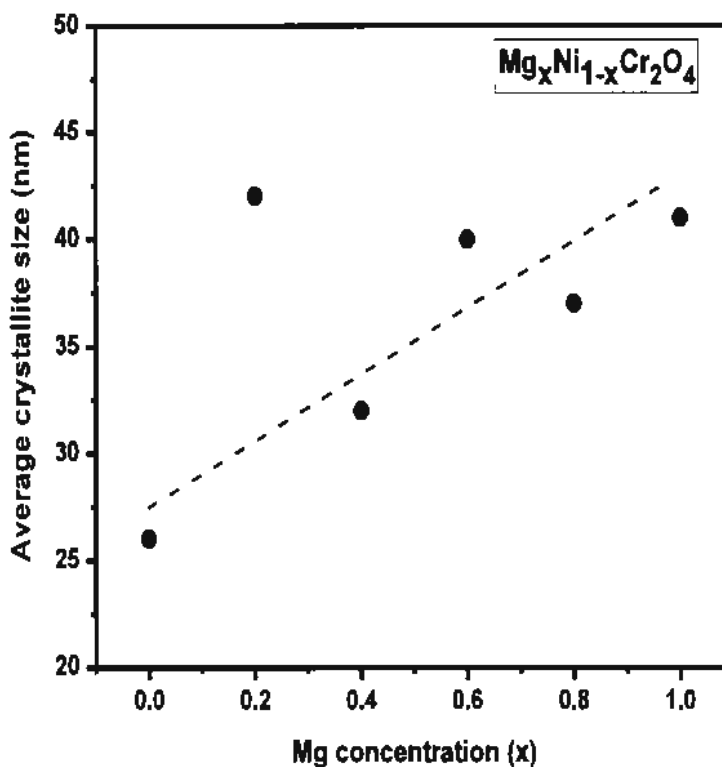
Fig. 4.3: Variation of average crystallite size with Mg concentration (x) of $Ni_{1-x}Mg_xCr_2O_4$ nanoparticles.

4.2   Transmission electron microscopy (TEM)

Transmission electron microscopy (TEM) was used to study the morphology, crystal size, and agglomeration. Fig. 4.4 shows the transmission electron microscopy image of $NiCr_2O_4$ nanoparticle at 100 nm scale. The TEM image shows that the nanoparticles are less agglomerated and non-spherical in shape [53].
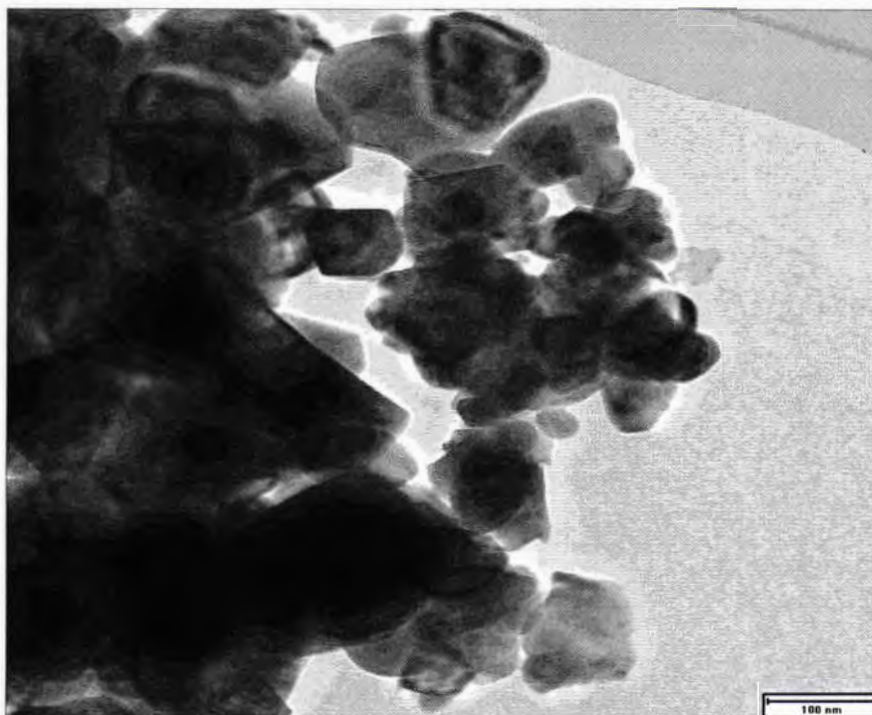
Fig. 4.4: TEM image of pure $NiCr_2O_4$ nanoparticles.

4.3   Fourier Transform Infrared spectroscopy

Fourier transform infrared spectroscopy (FTIR) is an important tool for measuring the optical properties of the polymeric, organic, and some inorganic materials.
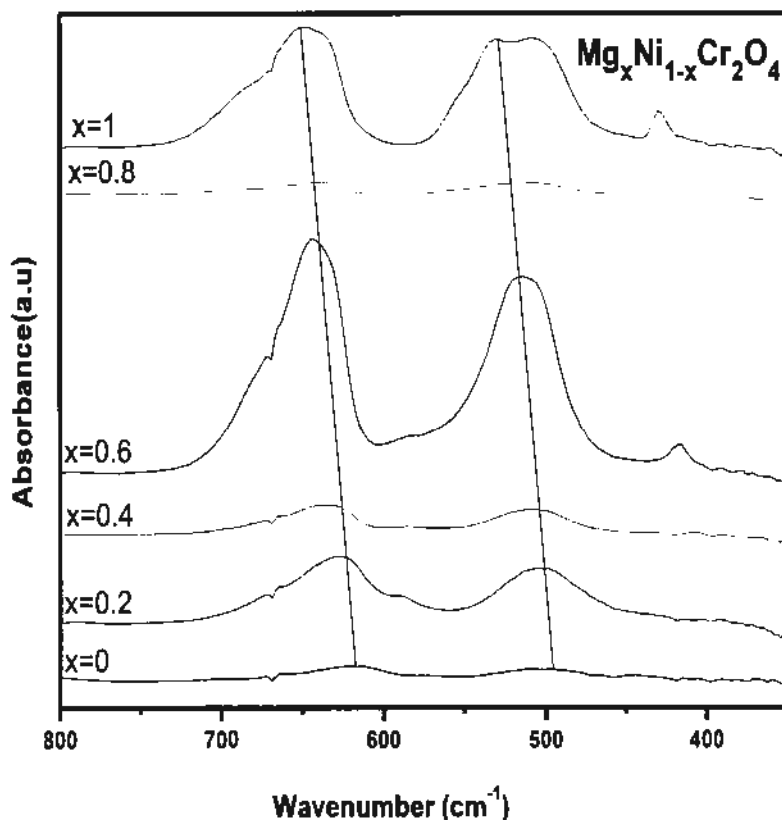
Fig. 4.5: FTIR of pure and Mg doped $NiCr_2O_4$ nanoparticles.

Fig. 4.5 shows the FTIR spectra of the different compositions of Mg in $NiCr_2O_4$ nanoparticles. It confirms the metal oxide bands. The vibration bands lies in the range 495 cm^{-1} to 530 cm^{-1} and 617 cm^{-1} to 651 cm^{-1} which confirm the formation of spinel ferrites [52]. In this spectrum, the absorption at 615 cm^{-1} and 496 cm^{-1} are the characteristic peak of the $NiCr_2O_4$ and confirm the formation of Cr-O and Ni-O vibrational bonds. There is a shift towards higher wavenumber with the increase in Mg concentration (as indicated by an arrow in Fig. 4.5). Keny *et al.* [78] reported a shift of a tetrahedral band of Mg ferrite toward higher wavenumber as compared to the Zn ferrite. The shift of the O–Mtet.–O vibration band with increasing Mg concentration signifies the preference of Mg ions in tetrahedral lattice sites in addition to octahedral sites. Pradeep *et al.*[79] reported that the Mg^{2+} ions prefer both tetrahedral and octahedral sites in Mg ferrite nanoparticles.

Table 4.3: Absorption bands at different concentration of Mg in $CoCr_2O_4$ nanoparticles.

48

x=0	x=0.2	x=0.4	x=0.6	x=0.8	x=1	Vibrational bonds
495	501	504	517	521	529	Ni-O & Mg-O
617	623	626	640	643	651	Cr-O

4.4   Magnetic properties

SQUID magnetometer was used to measure the magnetic properties of $NiCr_2O_4$ nanoparticles. We have done basic magnetic characterization such as M-H loop and ZFC/FC curves for only $CoCr_2O_4$ nanoparticles to study the magnetic nature of the nanoparticles.

4.4.1 M-H loop

Fig. 4.6 shows the M-H loop of pure $NiCr_2O_4$ nanoparticles at temperature T=5 K. The value of saturation magnetization (M_s) is 4.65 emu/g and the value of coercivity (H_c) is observed 19407 Oe. The large value of H_c shows that nanoparticles of $NiCr_2O_4$ are hard magnetic nature [54].
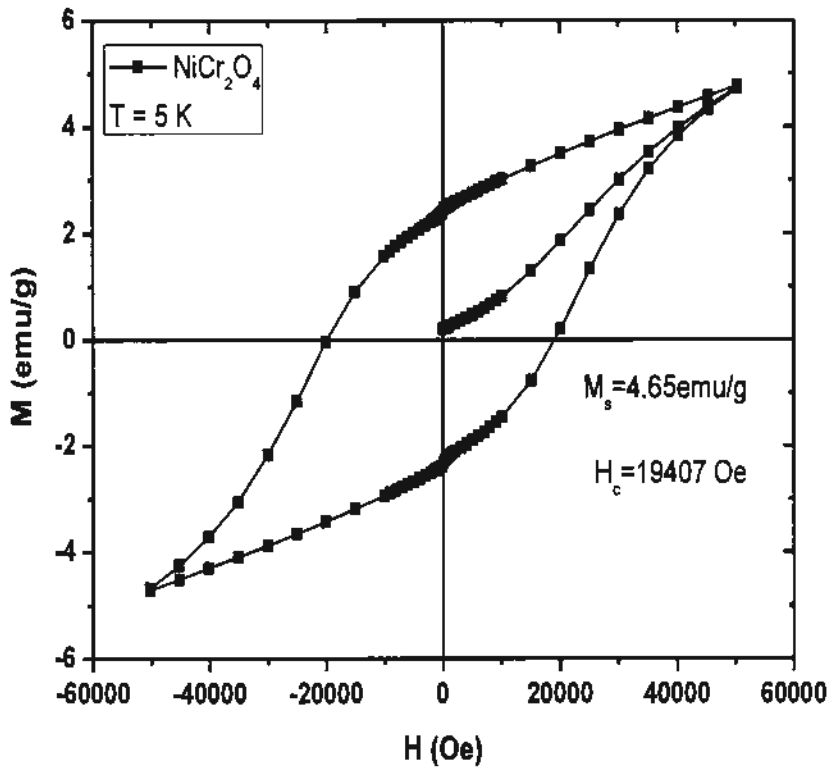
Fig. 4.6: M-H loop of $NiCr_2O_4$ nanoparticles at 5K.

4.4.2 Zero field cooled and Field cooled magnetization

For zero field cooled (ZFC) magnetic measurements, first the sample is cooled from 150 to 5 K under the absence of applied field. At 5 K, we applied 50 Oe field and measured the magnetization with increasing temperature. Fig. 4.7 shows the ZFC/FC curves of $NiCr_2O_4$ nanoparticles. The ZFC curve exhibits negative magnetization form 5 K to 18 K. The presence of negative magnetization value in the M (T) curves is related to the uncompensated spins in the nanoparticles. The nanoparticles exhibit a magnetic transition at 98 K which is referred as paramagnetic to ferrimagnetic transition for these kinds of nanoparticles. For FC measurements, we have applied the same 50 Oe field which was in the case of ZFC and then recorded the

magnetization while decreasing the temperature from 150 K to 5 K. Magnetization of FC curve

has been increased with applied field due to the alignment of magnetic moments in the direction

of applied field.

Fig. 4.7: Temperature dependent ZFC/FC of $NiCr_2O_4$ nanoparticles.

4.5   Dielectric properties

Materials that have capability to store energy when an electric field is applied are called

dielectric materials. The dielectric material can increase the charge storage capability of a capacitor

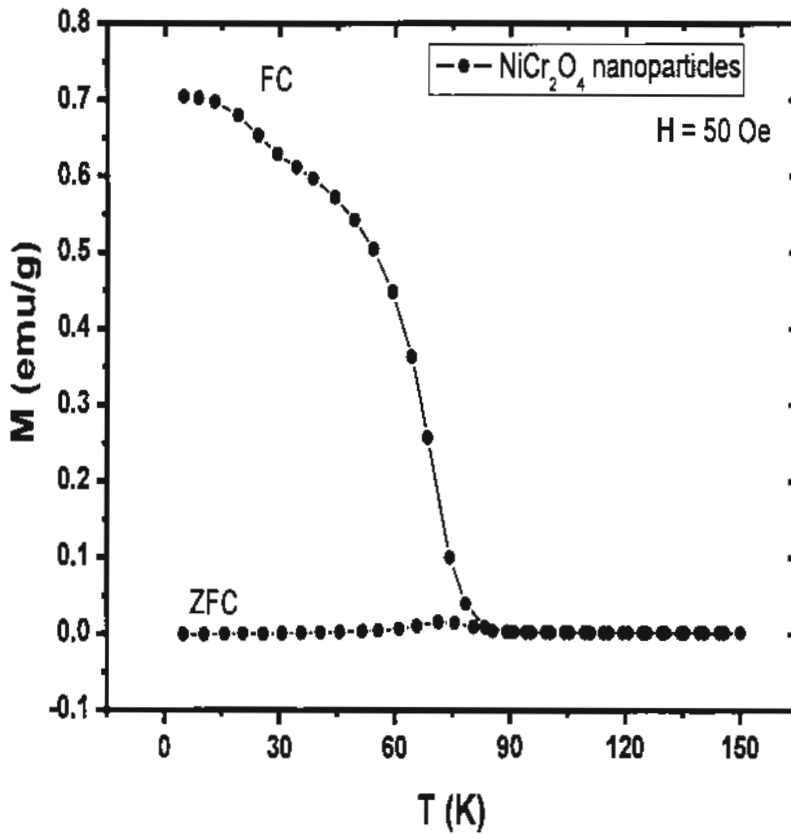and thus capacitance is strongly depending upon the dielectric constant. The formula to measure

dielectric constant is given below

$$\mathcal{E}' = \frac{Cd}{\mathcal{E}_0 A}$$ (4.5)

Here d is thickness of the pellet, $\mathcal{E}_0$ is permittivity, C is capacitance, A is the area of crossection.

The imaginary part of dielectric constant is calculated by the given relation.

$$\mathcal{E}'' = \mathcal{E}' \tan \delta$$ (4.6)

The dielectric properties of materials depend on frequency of applied field, temperature, crystal structure, cation distribution, grain size etc. Frequency dependent dielectric properties of $Mg_xNi_{1-x}Cr_2O_4$ nanoparticles with x = 0, 0.2, 0.4, 0.6, 0.8 and 1 were measured in the frequency range from 100 Hz to 5 MHz at room temperature. Fig. 4.8 (a) and Fig. 4.8 (b) shows real ($\mathcal{E}'$) and imaginary ($\mathcal{E}''$) part of dielectric constant, respectively. Both $\mathcal{E}'$ and $\mathcal{E}''$ exhibit maximum values at lower frequencies and decrease at higher frequencies. This is due to contribution of different types of polarization in different frequency regimes. In frequency range of 20 Hz to 3 M Hz, dipolar and interfacial polarizations play an important role in dielectric properties of chromites. The polarization mechanism in chromite spinel structure can be explained by electrical conduction process. Heikes and Johnston explained electrical conduction process with electron hopping model in material with spinel structure [80]. This model describes transferring of electrons in spinel structure within adjacent sites. Our sample is termed as a heterogeneous material, which have a granular nature, and contains pores. Grains and pores inside the material makes interfacial polarization effect prominent. This interfacial polarization effect is also called as Maxwell-Wagner effect or M-W Effect. According to this model, dielectric material is composed of grains and their grain boundaries. The grains are well conducting with poorly conducting grain boundaries. The electrons approach to the grain boundaries by hopping. Due to the highly resistive nature of the grain boundaries, electrons are stacked and produced polarization [81]. The decreasing trend of

52

dielectric constant (real and imaginary) with increasing frequency is due to lagging behind of space

charge carriers and they do not contribute in polarization. Therefore, the value of dielectric

constant decreases gradually with increasing frequency [82]. Values of ε' and ε'' at lower

frequencies sbow non-monotonous behavior with increasing Mg concentration and peaked at x =

0.2 as shown in insets of Fig. 4.8 (a) and (b), respectively. For nanoparticles with x = 0.2, resistive

grain boundaries exhibit more polarizability due to their larger average crystallite size as

compared to other Mg compositions, which results in a peak value of dielectric constant [83].

Interestingly, the variation of ε' and ε'' with x (as shown in inset of Fig. 4.8 (a)) nearly follows the

trend of average crystallite size with x (see Fig. 4.3), which employs that the dielectric properties

are more influenced by average crystallite size as compared to Mg concentration (x) in these

nanoparticles. At lower frequencies, the polarization effect is due to the interfacial and dipolar

polarization while at bigher frequencies electronic polarization play its role is polarization.
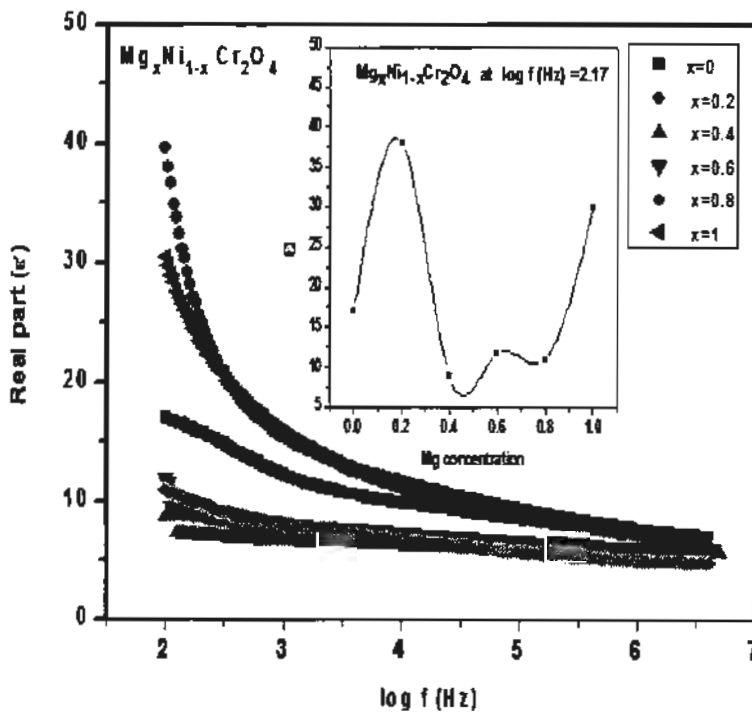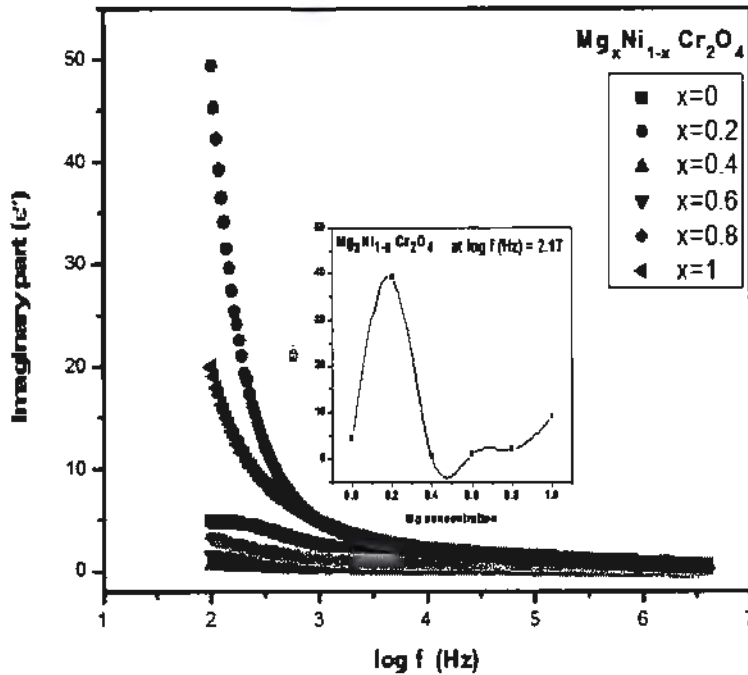
Fig. 4.8(a): Real and **(b)** imaginary part of dielectric constant of $Mg_xNi_{1-x}Cr_2O_4$ nanoparticles with x = 0, 0.2, 0.4, 0.6, 0.8 and 1. Insets shows the variation of real and imaginary parts with Mg concentration (x).

The tangent loss can be written as the ratio between the imaginary and real part of the dielectric constant. Tangent loss and loss factor are also known as the representation for energy absorption in a dielectric material. The power loss is defined as the Loss Tangent or tan δ and written as

$$\tan \delta = \frac{1}{2\pi f C_P R_P} \qquad (4.7)$$

Here R_p and C_p are the parallel resistance and parallel capacitance respectively.

The loss factor determines the loss in the material due to the damping of the dipoles moments vibrating inside a material. Fig. 4.9 shows the variation of tan δ as function of frequency for $Mg_xNi_{1-x}Cr_2O_4$ nanoparticles with x = 0, 0.2, 0.4, 0.6, 0.8, and 1 at room temperature. Tangent loss is maximum at lower frequency where the ability of storing charge is minimum. The variation of tangent loss with frequency can be also explained by Maxwell Wagner model [84-86]. The tangent loss also shows non-monotonous behaviour with Mg doping and the maximum loss factor is found for nanoparticles with x = 0.2 as shown in inset of Fig. 4.9. Other than this, there exists a conductivity loss. The collection of these two losses is called as loss tangent which depends on

54

frequency and determines that how much a material could be loss effective. The decrease in the tan δ at higher frequencies can be attributed to the losses accompanied by the vibrating and the conduction mechanism.
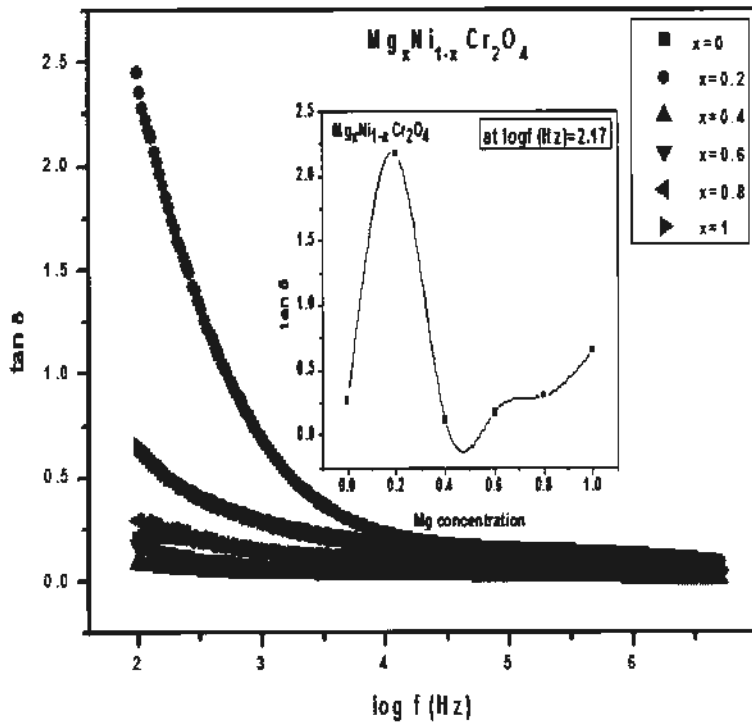
Fig. 4.9: Frequency dependence of tangent loss for $Mg_xNi_{1-x}Cr_2O_4$ (x = 0.0, 0.2, 0.4, 0.6,0.8 & 1.0) nanoparticles.

The tangent loss and loss factor are very important in determining the properties of the materials used in engineering. Electronics industry requires materials which show good electrical performance and are cost effective. Examples include desk-top computers, testing instruments and oscilloscopes which require fast signal processing systems.
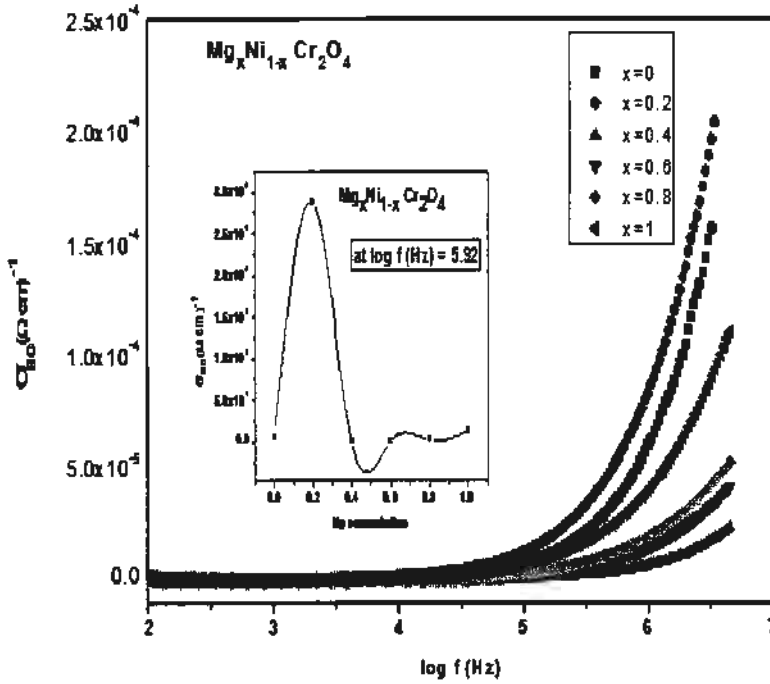
Fig. 4.10: Frequency dependent ac conductivity for $Mg_xNi_{1-x}Cr_2O_4$ (x = 0.0, 0.2, 0.4, 0.6, 0.8 & 1.0) nanoparticles.

A perfect dielectric material has neutral atoms and does not contain any free charge which could result in conduction of the current. The presence of free charge effects on the storage capability of the dielectric medium because a leakage current starts flowing. Every dielectric material contains some amount of free charge carriers and the resultant conductivity is explained by two factors which are dc conduction and ac conduction.

$$\sigma = \sigma_{d.c} + \sigma_{a.c} \qquad (4.8)$$

The $\sigma_{d.c}$ is measured from the bulk properties and defines the excitation of free electrons. This conduction can be measured by the Eq. 4.9:

$$\sigma_{d.c} = \frac{d}{R_b A} \qquad (4.9)$$

The d and A are the thickness and area of the pellets of our samples and R_b is the bulk resistance. The bulk resistance can be measured from the two probe method which is an application of Ohm's Law. Finally, the a.c conductivity can be measured from following Eq. 4.10:

56

$$\sigma_{a.c} = \mathcal{E}'\mathcal{E}_0\omega\tan\delta \qquad\qquad (4.10)$$

Here $\mathcal{E}'$ is dielectric constant, $\mathcal{E}_0$ is vacuum permittivity, ω is angular frequency ($2\pi f$) and finally tan δ is tangent loss. Fig. 4.9 shows the variation of ac conductivity as function of frequency for $Mg_xNi_{1-x}Cr_2O_4$ nanoparticles with x = 0, 0.2, 0.4, 0.6, 0.8, and 1. At low frequencies, it is nearly frequency independent while its value increases sharply at high frequencies. It is clear that conductivity increases as the frequency increases for each sample. The increase in trend with respect to increase in sintering temperature is also visible. This increasing trend can be explained by considering the sample as of grain nature with thin resistive layers of grain boundaries as predicted by Maxwell and Wagner model and also revealed by Koop's phenomenological theory. The grain boundaries have high resistance at low frequency region and as the frequency increases the grain effect becomes dominant and thus conductivity increases. Maximum ac conductivity is observed for largest grain size of nanoparticles with Mg concentration x = 0.2 as shown in inset of Fig. 4.9. From the dielectric study, it is concluded that the dielectric properties are enhanced for nanoparticles with x = 0.2 Mg concentration, however this effect is not due to Mg concentration but is related to average crystallite size (as the variation of dielectric parameters with x nearly follow the trend of average crystallite size with x as evident in Fig. 4.3). Therefore the dielectric properties are more influenced by average crystallite size than the Mg concentration in these Mg doped $NiCr_2O_4$ nanoparticles.

4.6   Conclusions

Single phase nano-crystalline $Mg_xNi_{1-x}Cr_2O_4$ ($x = 0.0, 0.2, 0.4, 0.6, 0.8$ and 1) nanoparticles have been successfully synthesized via sol-gel method. The average crystallite size was obtained by using Debye- Scherrer's formula lies in the range 26-42 nm for different concentration of Mg doped $NiCr_2O_4$ nanoparticles. X-ray diffraction (XRD) confirmed the cubic structure of $NiCr_2O_4$ and showed no impurity phases, which signifies the formation of single-phase $Ni_{1-x}Mg_xCr_2O_4$ nanoparticles. The average crystallite size showed an increasing trend with Mg concentration. Transmission electron microscopy (TEM) results confirmed that particles are less agglomerated and non-spherical in shape. Fourier transform infrared spectroscopy (FTIR) analysis showed two frequency bands as observed in the range of 495 to 530 cm^{-1} and 617 to 651 cm^{-1}, which are the characteristic peaks of $NiCr_2O_4$. M-H loop shows the value of saturation magnetization M_s is 4.65 emu/g which is less than the bulk value due to finite size effect and the value of coercivity is 19407 Oe proved that they are act as a hard magnet. ZFC curve exhibits negative magnetization form 5 K to 18 K which is due to uncompensated spins at grain boundaries. The frequency dependent dielectric studies were performed in a wide frequency range using an impedance analyzer. Dielectric parameters showed a non-monotonous behavior with Mg concentration and this behavior of dielectric parameters has been explained by using Koop's theory and Wagner's model. Dielectric measurements were enhanced with Mg doping and optimum value was found for $x = 0.2$ concentration which may be due to crystallite size and/or lattice constant.

References

[1] http://slideplayer.com/slide/4661608/.

[2] M.C. Roco, The long view of nanotechnology development: the National Nanotechnology Initiative at 10 years, in, Springer, 2011.

[3] O. Marti, B. Drake, S. Gould, P. Hansma, Atomic force microscopy and scanning tunneling microscopy with a combination atomic force microscope/scanning tunneling microscope, J. Vac. Sci. Technol., 6 (1988) 2089-2092.

[4] G. Binnig, H. Rohrer, Scanning tunneling microscopy, IBM J. Res. Dev., 44 (2000) 279.

[5] T. Harper, What is nanotechnology?, in, Iop publishing ltd dirac house, temple back, bristol bs16be, england, 2003.

[6] S. Chikazumi, Physics of magnetism, Wiley, 1964.

[7] A. Sabanovic, D.B. Izosimov, Application of sliding modes to induction motor control, IEEE Transactions on Industry Applications, (1981) 41-49.

[8] http://www.spring8.or.jp/en/news_publications/press_release/2013/130304-3/.

[9] J. Pople, Molecular-Orbital Theory of Diamagnetism. I. An Approximate LCAO Scheme, J. Chem. Phys., 37 (1962) 53-59.

[10] C.E. Hoyle, T. Watanabe, J.B. Whitehead, Anisotropic network formation by photopolymerization of liquid crystal monomers in a low magnetic field, Macromolecules, 27 (1994) 6581-6588.

[11] N. Brandt, S. Kuvshinnikov, A. Rusakov, V. Semenov, Anomalous diamagnetism (high-temperature meissner effect) in compound cucl, JETP Lett., 27 (1978) 33-38.

[12] http://slideplayer.com/slide/10908290/.

[13] A. Hiess, J. Boucherle, F. Givord, J. Schweizer, E. Lelievre-Berna, F. Tasset, B. Gillon, P. Canfield, Magnetism in intermediate-valence YbAl3: a polarized neutron diffraction study, J. Phys. Condens. Matter, 12 (2000) 829.

[14] W. Eerenstein, N. Mathur, J.F. Scott, Multiferroic and magnetoelectric materials, Nature., 442 (2006) 759.

[15] C. Benelli, A. Caneschi, D. Gatteschi, O. Guillou, L. Pardi, Synthesis, crystal structure, and magnetic properties of tetranuclear complexes containing exchange-coupled dilanthanide-dicopper (lanthanide= gadolinium, dysprosium) species, Inorg. Chem., **29** (1990) 1750-1755.

[16] http://hyperphysics.phy-astr.gsu.edu/hbase/Solids/ferro.html.

[17] M. Imada, A. Fujimori, Y. Tokura, Metal-insulator transitions, Rev. Mod. Phys., **70** (1998) 1039.

[18] https://www.doitpoms.ac.uk/tlplib/ferromagnetic/types.php.

[19] R.M. Cornell, U. Schwertmann, The iron oxides: structure, properties, reactions, occurrences and uses, John Wiley & Sons, 2003.

[20] http://physics.tutorvista.com/electricity-and-magnetism/properties-of-magnets.html.

[21] S. Hussain, S. Hussain, A. Waleed, M.M. Tavakoli, Z. Wang, S. Yang, Z. Fan, M.A. Nadeem, Fabrication of $CuFe_2O_4/\alpha-Fe_2O_3$ Composite Thin Films on FTO Coated Glass and 3-D Nanospike Structures for Efficient Photoelectrochemical Water Splitting, ACS Appl. Mater. Interfaces, **8** (2016) 35315-35322.

[22] G.G. Orenchak, Measuring soft ferrite core properties, in: Electrical Electronics Insulation Conference, 1995, and Electrical Manufacturing & Coil Winding Conference. Proceedings, IEEE, 1995, pp. 497-500.

[23] http://www.electronics-tutorials.ws/electromagnetism/magnetic-hysteresis.html.

[24] R. De Groot, F. Mueller, P. Van Engen, K. Buschow, New class of materials: half-metallic ferromagnets, Phys. Rev. Lett., **50** (1983) 2024.

[25] K.H.J. Buschow, F.R. Boer, Physics of magnetism and magnetic materials, Springer, 2003.

[26] A.S. GENE, structural, optical and magnetic characterization of spinel zinc chromite $(ZnCr_2O_4)$ nanocrystals synthesized by thermal treatment method, in, school of graduate studies, universiti putra malaysia, 2014.

[27] J.K. Burdett, G.L. Rosenthal, The factors influencing coordination numbers in solids, J. Solid State Chem., **33** (1980) 173-180.

[28] D.C. Culita, C.M. Simonescu, M. Dragne, N. Stanica, C. Munteanu, S. Preda, O. Oprea, Effect of surfactant concentration on textural, morphological and magnetic properties of $CoFe_2O_4$ nanoparticles and evaluation of their adsorptive capacity for Pb (II) ions, Ceram. Int., **41** (2015) 13553-13560.

[29] M.T. Rahman, C. Ramana, Gadolinium-substitution induced effects on the structure and AC electrical properties of cobalt ferrite, Ceram. Int., **40** (2014) 14533-14536.

[30] R. Nongjai, S. Khan, K. Asokan, H. Ahmed, I. Khan, Magnetic and electrical properties of In doped cobalt ferrite nanoparticles, J. Appl. Phys., **112** (2012) 084321.

[31] S. Ziemniak, A. Gaddipati, P. Sander, Immiscibility in the $NiFe_2O_4$–$NiCr_2O_4$ spinel binary, J. Phys. Chem. Solids, **66** (2005) 1112-1121.

[32] G.T. Anand, L.J. Kennedy, J.J. Vijaya, Microwave combustion synthesis, structural, optical and magnetic properties of $Zn_{1-x}Co_xAl_2O_4$ ($0 \leqslant x \leqslant 0.5$) spinel nanostructures, J. Alloys Compd., **581** (2013) 558-566.

[33] https://physics.stackexchange.com/questions/89157/motion-of-a-dipole-in-an-electric-field.

[34] J.W.D. Callister, Chapter 11 Applications and Processing of Metal Alloys, Material Science and Engineering an Introduction, 7th ed., John Wiley & Sons, Inc, (2007) 364-365.

[35] https://eng.libretexts.org/Core/Materials_Science/Optical_Properties/Dielectric_Polarization.

[36] C.P. Smyth, Dielectric polarization and relaxation, Annu. Rev. Phys. Chem., **17** (1966) 433-456.

[37] N. Ashcroft, N. Mermin, Solid State Physics, ch. 2, Pacific Grove: Brooks/Cole, (1976) 29-55.

[38] http://www.chegg.com/homework-help/consider-atom-presence-oscillating-electric-field-figure-94-chapter-9-problem-8-solution-9780073104645-exc.

[39] https://www.tf.uni-kiel.de/matwis/amat/elmat_en/kap_3/backbone/r3_2_3.html.

[40] R. Rajput, Thermal engineering, Laxmi Publications, 2010.

[41] https://www.americanpiezo.com/piezo-theory/piezoelectricity.html.

[42] A.S. Kumar, P. Suresh, M.M. Kumar, H. Srikanth, M. Post, K. Sahner, R. Moos, S. Srinath, Magnetic and ferroelectric properties of Fe doped $SrTiO_{3-\delta}$ films, in: J. Phys. Conf. Ser. , IOP Publishing, 2010, pp. 092010.

[43] https://www.slideshare.net/Mohd_Limdi/dielectrics-and-its-applications.

[44] D.R. Askeland, P.P. Phulè, The Science and Engineering of Materials, Brooks/Cole, Cerca con Google, (2003).

[45] http://nptel.ac.in/courses/113104005/lecture18a/18_2.htm.

[46] H. Fröhlich, A. Taylor, The boltzmann equations in electron-phonon systems, Proceedings of the Physical Society, **83** (1964) 739.

[47] N.-H. Li, Y.-H. Chen, C.-Y. Hu, C.-H. Hsieh, S.-L. Lo, Stabilization of nickel-laden sludge by a high-temperature $NiCr_2O_4$ synthesis process, J. Hazard Mater., **198** (2011) 356-361.

[48] F. Beshkar, M. Salavati-Niasari, Facile synthesis of nickel chromite nanostructures by hydrothermal route for photocatalytic degradation of acid black 1 under visible light, J. Nanostruct., **5** (2015) 17-23.

[49] S.K. Durrani, S. Naz, M. Mehmood, M. Nadeem, M. Siddique, Structural, impedance and Mössbauer studies of magnesium ferrite synthesized via sol–gel auto-combustion process, J. Saudi Chem. Soc., (2016).

[50] Y. Choi, J. Okamoto, D. Huang, K. Chao, H. Lin, C. Chen, M. Van Veenendaal, T. Kaplan, S. Cheong, Thermally or magnetically induced polarization reversal in the multiferroic $CoCr_2O_4$, Phys. Rev. Lett., **102** (2009) 067601.

[51] A. Bush, V.Y. Shkuratov, K. Kamentsev, V. Cherepanov, Preparation and X-ray diffraction, dielectric, and Mössbauer characterization of $Co_{1-x}Ni_xCr_2O_4$ solid solutions, Inorg. Mater., **49** (2013) 296-302.

[52] M. Enhessari, A. Salehabadi, S. Khanahmadzadeh, K. Arkat, J. Nouri, Modified Sol-Gel Processing of $NiCr_2O_4$ Nanoparticles; Structural Analysis and Optical Band Gap, High Temp. Mat. Pr., **36** (2017) 121-125.

[53] S.A. Bakar, N. Soltani, W.M.M. Yunus, E. Saion, A. Bahrami, Structural and paramagnetic behavior of spinel $NiCr_2O_4$ nanoparticles synthesized by thermal treatment method: Effect of calcination temperature, Solid State Commun., **192** (2014) 15-19.

[54] J. Barman, T. Bora, S. Ravi, Study of exchange bias and training effect in $NiCr_2O_4$, J. Magn. Magn. Mater., **385** (2015) 93-98.

[55] M. Ptak, M. Maczka, A. Gągor, A. Pikul, L. Macalik, J. Hanuza, Temperature-dependent XRD, IR, magnetic, SEM and TEM studies of Jahn–Teller distorted $NiCr_2O_4$ powders, J. Solid State Chem., **201** (2013) 270-279.

[56] X. Liu, N. Yin, T. Thomas, M. Yang, J. Wang, Q. Shi, Effect of nitrogen substitution on the structural and magnetic ordering transitions of $NiCr_2O_4$, RSC Advances, 6 (2016) 112140-112147.

[57] A. Mantlikova, J.P. Vejpravova, P. Holec, J. Plocek, D. Niznansky, Magnetic properties of TCr_2O_4 (T= Co, Ni) fine powders and TCr_2O_4/SiO_2 nanocomposites, in: Mater. Sci. Eng., IOP Publishing, 2011, pp. 032022.

[58] T. Rudolf, C. Kant, F. Mayr, J. Hemberger, V. Tsurkan, A. Loidl, Spin-phonon coupling in antiferromagnetic chromium spinels, New J. Phys, 9 (2007) 76.

[59] M. Terada, T. Maekawa, The infrared absorption spectra of several chromites, J. **Japan Inst. Metals, 5** (1964) 205-206.

[60] C.L. Honeybourne, R.K. Rasheed, Nitrogen dioxide and volatile sulfide sensing properties of copper, zinc and nickel chromite, J. Mater. Chem., 6 (1996) 277-283.

[61] N. Mufti, A. Nugroho, G. Blake, T. Palstra, Magnetodielectric coupling in frustrated spin systems: the spinels MCr_2O_4 (M= Mn, Co and Ni), J. Phys. Condens. Matter, 22 (2010) 075902.

[62] O. Crottaz, F. Kubel, H. Schmid, Jumping crystals of the spinels $NiCr_2O_4$ and $CuCr_2O_4$, J. Mater. Chem., 7 (1997) 143-146.

[63] https://str.llnl.gov/str/May05/Satcher.html.

[64] B. Sivasankar, Engineering chemistry, Tata McGraw-Hill New Delhi, 2008.

[65] B. Cullity, Elements of XRD, USA Edison-Wesley P Inc, (1978).

[66]https://www.slideshare.net/bharathpharmacist/81347482-xraydiffractiontechnique-39635806.

[67] https://commons.wikimedia.org/wiki/File:Bragg%27s_Law.PNG.

[68] http://slideplayer.com/slide/5266507/.

[69] R. Wahab, S. Ansari, Y. Kim, H. Seo, G. Kim, G. Khang, H.-S. Shin, Low temperature solution synthesis and characterization of ZnO nano-flowers, Mater Res Bull., 42 (2007) 1640-1648.

[70] http://pd.chem.ucl.ac.uk/pdnn/diff2/kinemat2.htm.

[71] http://www.mechanicalengineeringblog.com/153-x-ray-diffraction-crystal-structure/.

[72] https://en.wikipedia.org/wiki/2006.

[73] http://www.ufrgs.br/imunovet/molecular_immunology/microscopy.html.

[74] https://en.wikibooks.org/wiki/Special_Relativity/Aether.

[75] http://hyperphysics.phy-astr.gsu.edu/hbase/Solids/Squid.html.

[76] https://www.wmi.badw.de/methods/squid.htm.